

1 **A new model for the global biogeochemical cycle of carbonyl**  
2 **sulfide. Part 1: Assessment of direct marine emissions with an**  
3 **oceanic general circulation and biogeochemistry model**

4  
5 **T. Launois<sup>1</sup>, S. Belviso<sup>1</sup>, L. Bopp<sup>1</sup>, C.G. Fichot<sup>2</sup> and P. Peylin<sup>1</sup>**

6 [1] Laboratoire des Sciences du Climat et de l'Environnement (LSCE Saclay), IPSL, CEA,  
7 CNRS, UVSQ, CE Saclay, Bât 703 L'Orme des Merisiers, 91191, Gif-sur-Yvette, France

8 [2] Jet Propulsion Laboratory, California Institute of Technology, Pasadena, California, USA

9  
10 Correspondence to: T. Launois (thomas.launois@lsce.ipsl.fr)

11  
12 **Abstract**

13 The global budget of tropospheric carbonyl sulfide (OCS) is believed to be at equilibrium  
14 because background air concentrations have remained roughly stable over at least the last  
15 decade. Since the uptake of OCS by leaves (associated to photosynthesis) and soils have been  
16 revised significantly upwards recently, an equilibrated budget can only be obtained with a  
17 compensatory source of OCS. It has been assumed that the missing source of OCS comes  
18 from the low-latitude ocean, following the incident solar flux. The present work uses  
19 parameterizations of major production and removal processes of organic compounds  
20 in the NEMO-PISCES Ocean General Circulation and Biogeochemistry Model to assess the  
21 marine source of OCS. In addition, the OCS photo-production rates computed  
22 with the NEMO-PISCES model were evaluated independently using the UV absorption  
23 coefficient of chromophoric dissolved organic matter (derived from satellite ocean color) and  
24 apparent quantum yields available in the literature. Our simulations show global direct marine  
25 emissions of OCS in the range of 573-3997 GgS yr<sup>-1</sup>, depending mostly on the quantification  
26 of the absorption rate of chromophoric dissolved organic matter. The high estimates on that  
27 range are unlikely, as they correspond to a formulation that most likely overestimate photo-  
28 production process. Low and medium (813 GgS yr<sup>-1</sup>) estimates derived from the NEMO-  
29 PISCES model are however consistent spatially and temporally with the suggested missing  
30 source of Berry et al. (2013), allowing thus to close the global budget of OCS given the recent  
31 estimates of leaf and soil OCS uptake.

## 1 **1 Introduction**

2 Carbonyl sulfide (OCS) is a long-lived sulfur-containing trace gas with direct and indirect  
3 effects on the radiation budget of the atmosphere (OCS being both a tropospheric greenhouse  
4 gas and a source of sulfur aerosols to the stratosphere). But these radiative effects are low  
5 compared to the radiative forcings of greenhouse gases (GHG) and tropospheric aerosols of  
6 anthropogenic origin (Brühl et al., 2012 and references therein). But because OCS is the most  
7 abundant sulfur-containing gas in the atmosphere, it is a major contributor to the stratospheric  
8 sulfate layer during volcanically quiescent periods (Notholt et al., 2003). OCS also  
9 participates in some key reactions within the global carbon cycle, especially reactions  
10 associated with leaf photosynthesis and soil microbial activities (Berry et al., 2013 and  
11 references therein). As such, it holds great promises for the studies of plant physiology,  
12 terrestrial ecosystem production and the global carbon cycle thanks to its potential use as a  
13 tracer for canopy photosynthesis, transpiration and stomatal conductance (Wohlfahrt et al.,  
14 2012 and references therein).

15 Measurements of OCS from the global air-monitoring network of the National Oceanic and  
16 Atmospheric Administration (NOAA) provided compelling evidence for the existence of a  
17 major sink of this gas in the continental boundary layer, mainly attributed to biospheric uptake  
18 (Montzka et al., 2007; Campbell et al., 2008). The uptake of OCS by plants was modeled to  
19 be no more than 240 GgS yr<sup>-1</sup> by Kettle et al. (2002), but it has been recently revised upwards,  
20 with new estimates of 490 GgS yr<sup>-1</sup> (Suntharalingam et al., 2008), of 738 GgS yr<sup>-1</sup> in the work  
21 of Berry et al. (2013) and even reaching up to 1500 GgS yr<sup>-1</sup> in Montzka et al. (2007). Soils  
22 could also play a role in the budget of OCS. It is still a strong matter of debate but recent  
23 estimates suggest that much more OCS is taken up by soils than proposed by Kettle et al.  
24 (2002) (355 GgS yr<sup>-1</sup>, according to Berry et al., 2013, compared with an estimate of around  
25 130 GgS yr<sup>-1</sup> in Kettle et al., 2002). Since background air concentrations have remained  
26 roughly stable over at least the last decade (Montzka et al., 2007), the global budget of  
27 tropospheric OCS is believed to be at equilibrium. Kettle et al. (2002) proposed a global  
28 budget of OCS with ocean and anthropogenic sources compensating for the main uptake by  
29 vegetation. However, because deposition fluxes of OCS to vegetation and soils are three times  
30 higher than proposed in the study by Kettle et al. (2002), an equilibrated budget can only be  
31 obtained with a compensatory source of OCS. Berry et al. (2013) suggests that the missing  
32 source of OCS comes from the oceans. This missing source has been inferred through a  
33 simple inversion approach that optimizes sources and sinks based on global measurements of

1 atmospheric OCS mixing ratios collected in the NOAA network. This inversion pointed  
2 towards a larger global oceanic source of OCS with higher proportions of tropical emissions  
3 than previously established.

4 The ocean is believed to be the largest source of atmospheric OCS (Chin and Davis, 1993;  
5 Kettle et al., 2002; Berry et al., 2013). It contributes to OCS in the troposphere by direct  
6 emission of this gas, and by large emissions of carbon disulfide (CS<sub>2</sub>) and dimethylsulfide  
7 (DMS) quickly oxidized into OCS (with an approximate lifetime of 1 day) (Barnes et al.,  
8 1994; Kloster, 2006). Barnes et al. (1994) suggested that OCS accounts for 0.7% of the  
9 oxidation products of DMS, and that 87% of the marine emissions of CS<sub>2</sub> are converted into  
10 OCS. However, estimates of sea-air fluxes of OCS and their spatial distributions remain  
11 largely unknown. Kettle et al. (2002) simulated direct global oceanic OCS fluxes from -110  
12 GgS yr<sup>-1</sup> (a sink) to 190 GgS yr<sup>-1</sup> (a source to the atmosphere), while previous estimates based  
13 on field observations suggested global direct oceanic OCS emissions from 160 to 640 GgS yr<sup>-1</sup>  
14 (Chin and Davis, 1993; Watts, 2000). The Kettle et al. (2002) study suggested that direct  
15 sea-air OCS emissions mainly take place at mid and high latitudes, during the respective  
16 periods of maximum irradiance.

17 OCS surface concentrations show a strong diurnal cycle with a mid-afternoon maximum,  
18 suggesting that photo-production is a major source of marine OCS (Ferek and Andreae, 1984;  
19 Xu et al., 2001; Von Hobe et al., 2003). In addition, OCS can also be produced in marine  
20 waters when no light is available. This pathway is therefore called dark-production.  
21 Measurements by Von Hobe et al. (2001) indicated that its rate is proportional to the amount  
22 of organic material, and it has therefore so far been linked to the chromophoric dissolved  
23 organic matter (CDOM) absorption coefficient (Von Hobe et al., 2001 and 2003). Finally,  
24 OCS surface concentrations and fluxes are also strongly influenced by the continuous  
25 temperature- and pH-dependent hydrolysis of OCS to carbon dioxide (CO<sub>2</sub>) and hydrogen  
26 sulfide (H<sub>2</sub>S) (Von Hobe et al., 2003).

27 The present work reassesses the marine source of OCS using the 3D oceanic NEMO-PISCES  
28 Ocean General Circulation and Biogeochemistry model with process-based parameterizations  
29 of the main OCS production and removal processes (Fig. 1). The present study proposes two  
30 independent approaches to quantify the photo-production of OCS. The dark-production rate  
31 implemented in the NEMO-PISCES model follows the formulation of Von Hobe et al. (2001,  
32 2003). Therefore, the dark-production rate, even if supposed to be light-independent, is also  
33 linked to the chromophoric dissolved organic matter absorption coefficient at 350nm ( $a_{350}$ ), as

1 the variable provides an indirect estimate of the seawater richness in organic matter. As  
2 parameterizations found in literature for both dark- and photo-production of OCS are related  
3 to the UV absorption coefficient of CDOM at 350 nm, sensitivity tests are performed using  
4 three different formulations for this variable. Sensitivity tests are also performed on  
5 hydrolysis, exploring two different formulations. Global maps of OCS concentrations  
6 obtained with the NEMO-PISCES model are compared with in-situ measurements. Finally,  
7 the magnitude and spatial distributions of global OCS emissions modeled in the present work  
8 are compared to previous global estimates.

9

## 10 **2 Methods**

### 11 **2.1 Description of NEMO-PISCES and experimental design**

12 In this study, we use the Pelagic Interaction Scheme for Carbon and Ecosystem Studies  
13 (PISCES) ocean biogeochemical model. As a detailed description of the model  
14 parameterizations is given in Aumont and Bopp (2006), the model is only briefly presented  
15 here. The model has 24 compartments, including four living pools: two phytoplankton size  
16 classes/groups (nanophytoplankton and diatoms) and two zooplankton size classes  
17 (microzooplankton and mesozooplankton). Phytoplankton growth can be limited by five  
18 different nutrients: nitrate, ammonium, phosphate, silicate and iron. The internal  
19 concentrations of chlorophyll for both phytoplankton groups are prognostically simulated  
20 with Chlorophyll-to-Carbon ratios computed as a function of light and nutrient stress. There  
21 are three nonliving compartments: semi-labile dissolved organic matter (with remineralization  
22 timescales of several weeks to several years), small and large sinking particles. In addition to  
23 the version of the model used in Aumont and Bopp (2006), we also include here a prognostic  
24 module computing OCS concentrations in seawater.

25 PISCES is coupled to the general circulation model Nucleus for European Modelling of the  
26 Ocean (NEMO, Madec et al. 1998). A release of the model is available for the community  
27 (<http://www.nemo-ocean.eu/>). Here, we use the global configuration ORCA2 with a  
28 resolution of  $2^\circ \times 0.5\text{-}2^\circ$  and 31 vertical levels (with a  $\sim 10\text{m}$ -resolution in the first 200m).  
29 NEMO-PISCES is first run 3,000 years to obtain an equilibrated state, forced in offline mode  
30 by the Consortium for Oceanic Research and Education (CORE2) Normal Year Forcing,  
31 (Large and Yeager (2008)) and initialized with climatological nutrient data. The OCS module  
32 is then only run two additional years as it converges towards equilibrium much more rapidly.  
33 The results presented in this study correspond to the last year of this simulation.

34

## 1 **2.2 Parameterizations of OCS production and removal processes implemented in** 2 **NEMO-PISCES**

3 The clear diurnal cycle of sea-surface OCS concentrations with peak values during mid-  
4 afternoon suggests photochemical processes play an important role in the production of OCS.  
5 Organo-sulfur compounds with thiol groups (-SH), such as cysteine and methyl mercaptans  
6 (CH<sub>3</sub>SH), have been suggested as OCS precursors (Ferek and Andreae, 1984; Flöck et al.,  
7 1997; Ulshöfer et al., 1996). Moreover, measured CH<sub>3</sub>SH diurnal cycles were coherent with  
8 the hypothesis that its photo-destruction could lead to OCS production (Xu et al., 2001).  
9 Because no global map of CH<sub>3</sub>SH is available, we followed parameterizations of OCS photo-  
10 production found in literature which relate photo-production rate of OCS to the UV irradiance  
11 intensity at the sea surface and to the efficiency of chromophoric dissolved organic matter  
12 (CDOM) available to absorb this UV radiation. The quantification of this photochemical  
13 process can be amenable to remote sensing because of its critical dependence on ocean UV  
14 and visible optical properties. Additional parameterizations were needed to complete the  
15 description of OCS formation and destruction processes in NEMO-PISCES. We therefore  
16 implemented specific equations to calculate the formation of OCS via dark-production (a  
17 light-independent pathway) and the hydrolysis rate of OCS in sea waters. Finally, air-sea  
18 exchanges of OCS were described in an analogous way to Fick's diffusion law.

### 19 **2.2.1 UV light penetration in seawater:**

20 In NEMO-PISCES, surface irradiance received at each grid point is a function of cloud  
21 coverage and deduced surface UV irradiance is taken equal to 4.4% of the total light received  
22 at sea surface. UV penetration at depth in marine waters in NEMO-PISCES was taken equal  
23 to the penetration calculated with the deep blue wavelength for visible light attenuation  
24 coefficient. As this is a rough approximation and might lead to over-estimating maximum  
25 depth penetration for UV irradiance, we set the UV value to zero for layers deeper than 30 m,  
26 which corresponds to the average depth at which less than 10% of surface UV irradiance  
27 penetrates for marine waters containing less than 1 mg m<sup>-3</sup> of chlorophyll (Bricaud et al.,  
28 1995; Tedetti et al., 2007).

### 29 **2.2.2 Parameterization of CDOM absorption coefficient at 350 nm ( $a_{350}$ )**

30 Chromophoric (or colored) dissolved organic matter (CDOM) is the fraction of the dissolved  
31 organic matter that absorbs light, ranging from ultraviolet to visible wavelengths. CDOM has  
32 been identified as one of the most influential factors to control UV attenuation in waters. Its  
33 concentration increases in seawater with elevated biological production rates and terrestrial

1 inputs. CDOM distribution is also controlled by the deep ocean circulation, upwelling and/or  
2 vertical mixing (Para et al., 2010 and references therein). Its concentration decreases with  
3 photochemical degradation and microbial consumption. CDOM absorbs part of available  
4 light, therefore negatively impacting primary productivity of aquatic ecosystems. However, as  
5 provider of a substitute for microbial respiration, photo-degraded CDOM positively impacts  
6 the secondary productivity of the oceanic ecosystems.

7 As no reliable parameterization is currently available to calculate CDOM concentrations, due  
8 to insufficient knowledge on the controlling processes of CDOM formation and destruction,  
9 we chose to follow the study from Para et al. (2010) and assumed that the CDOM absorption  
10 at 350nm ( $a_{350}$ ) was a good indicator of CDOM concentrations. The wavelength of 350nm  
11 was chosen because it corresponds to the maximum sensitivity of the Eppley UV light sensors  
12 used during the marine campaigns where links between CDOM concentration, CDOM  
13 absorption and OCS production were established (Uher et al., 1997; Preiswerk et al., 2000).  
14 This wavelength has also been proven to be the most efficient for the photochemical  
15 excitation of dissolved organic matter (Farmer et al., 1993). OCS production is either  
16 dependent on irradiance in the UV domain (photo-production) or on CDOM and organic  
17 matter concentration (dark-production). As  $a_{350}$  allows a link with both variables, it is a key  
18 parameter in our parameterizations of OCS production. Sensitivity tests were performed using  
19 NEMO-PISCES and three different formulations of  $a_{350}$ .

20 The first two formulations of CDOM absorption coefficients were proposed by Morel and  
21 Gentili (2009) and Preiswerk et al. (2000), who deduced them at a given wavelength from in  
22 situ measurements, and then extrapolated the absorption coefficient of CDOM at 350 nm by  
23 using the following standard exponential relation:

$$24 \quad a_{CDOM}(\lambda) = a_{CDOM}(\text{ref}) * e^{(-S*(\text{ref}-\lambda))} \quad (1)$$

25 where S is the spectral slope coefficient of CDOM between  $\lambda$  and the reference wavelength  
26 (ref).

#### 27 **a) $a_{350}$ from Morel and Gentili (2009)**

28 The parameterization of  $a_{350}$  from Morel and Gentili (2009) is based on spectral reflectances  
29 of the ocean over Case 1 waters. Case 1 waters are those for which the optical properties of  
30 CDOM closely follow the optical properties of phytoplankton, as defined in Morel (1988).  
31 Spectral reflectances were derived from ocean color remote sensing data at several  
32 wavelengths to allow separation between CDOM and chlorophyll reflectance signatures.

1 Products from SeaWiFS monthly global composites for the 2002-2007 period were used, and  
 2 led to the following relation between CDOM absorption coefficient and chlorophyll  
 3 concentration:

$$a_{CDOM}(400) = 0.065[\text{Chl}]^{0.63} \quad (2)$$

4 **b)  $a_{350}$  from Preiswerk et al. (2000)**

5 The second parameterization was taken from Preiswerk et al. (2000) who deduced  $a_{350}$  from  
 6 modeled CDOM absorption coefficient at 440 nm. To model  $a_{440}$ , satellite ocean color data  
 7 were used as a proxy for chlorophyll concentration and combined with the relation of Garver  
 8 and Siegel (1998), Eq. (3):

$$\text{per}(a_{440}) = -26 [\log(\text{chl})] + 26 \quad (3)$$

$$a_{PH,440} = 0.0448\text{chl} \quad (4)$$

$$\text{per}(a_{440}) = \frac{a_{440}}{a_{PH,440} + a_{440}} * 100\% \quad (5)$$

12 where  $a_{PH,440}$  is the absorption coefficient of the phytoplankton at 440 nm, and  $\text{per}(a_{440})$  is  
 13 the percent of the total non-seawater absorption coefficient at 440 nm (due to CDOM).

14 **c)  $a_{350}$  from MODIS *Aqua* ocean color**

15 A relationship between  $a_{350}$  and chlorophyll-a was established independently, using MODIS  
 16 *Aqua* ocean color data collected continuously between July 2002 and July 2010. Monthly  
 17 climatologies of MODIS *Aqua* chlorophyll-a surface concentrations were used, and MODIS  
 18 *Aqua* remote-sensing reflectances were used to derive corresponding monthly climatologies  
 19 of  $a_{350}$  for the global surface ocean. The SeaUV algorithm developed by Fichot et al. (2008)  
 20 was used to estimate the diffuse attenuation coefficient at 320 nm,  $K_d(320)$ , from the remote-  
 21 sensing reflectances. A ratio  $a_{CDOM}(320)/K_d(320) = 0.68$  derived from an extensive set of in  
 22 situ measurements was then used to calculate the absorption coefficient of CDOM at 320 nm,  
 23  $a_{320}$ , from  $K_d(320)$  (Fichot and Miller, 2010). A spectral slope coefficient of 0.0198 derived  
 24 from the same *in situ* data set was then used to calculate  $a_{350}$  from  $a_{320}$  using Eq. (1).

25 The  $a_{350}$  data from the twelve monthly climatologies were regressed on the corresponding  
 26 MODIS *Aqua* chlorophyll-a concentrations using the fourth-order polynomial shown in Eq.  
 27 (6).

$$\ln(a_{350}) = 0.5346C - 0.0263C^2 - 0.0036C^3 + 0.0012C^4 - 1.6340 \quad (6)$$

29 where C is the chlorophyll concentration in  $\text{mg m}^{-3}$ , and  $a_{350}$  has units of  $\text{m}^{-1}$ .

30 The equation 6 was then added in NEMO-PISCES to complete the sensitivity tests of the  
 31 OCS concentrations on the different  $a_{350}$  expressions tested.

### 1 2.2.3 OCS photo-production rates as modeled in NEMO-PISCES

2 OCS photo-production is primarily induced by the interaction of UV radiation and natural  
3 photosensitizers in CDOM (Ferek and Andreae, 1984; Flöck et al., 1997). Therefore, the Uher  
4 et al. (1997) photo-production parameterization takes into account both the incident UV  
5 irradiance and OCS production efficiency (apparent quantum yield, AQY). An AQY  
6 represents the spectral efficiency of a photochemical process (e.g., photochemical production  
7 of OCS), and is generally determined in the laboratory by normalizing the quantity of OCS  
8 produced during solar exposure to the amount of photons absorbed by CDOM during that  
9 same solar exposure. The resulting expression for photoproduction rate proposed is:

$$10 \quad P = p \, UV \quad (7a)$$

11 where  $P$  is the OCS photo-production rate,  $p$  a zeroth-order photoproduction constant ( $\text{fmol L}^{-1}$   
12  $\text{s}^{-1} \text{W}^{-1} \text{m}^2$ ) and  $UV$  the solar UV light density.

13 This expression was established using strong assumptions, such as considering that no other  
14 source or sink of OCS affects OCS concentration in seawaters. In their study, Uher et al.  
15 (1997) measured mean values for the photoproduction constant  $p$  around  $1.3 \pm 0.3 \text{ fmol L}^{-1} \text{ s}^{-1}$   
16  $\text{W}^{-1} \text{m}^2$  on offshore samples and values twice as high in inshore waters, around  $2.8 \pm 0.3 \text{ fmol}$   
17  $\text{L}^{-1} \text{ s}^{-1} \text{W}^{-1} \text{m}^2$  (all measurements done in April 1993, in the North Sea).

18 A few AQY for OCS have been published, but they exhibit considerable variability, with  
19 values varying by a factor of  $>7$  depending on the environment considered (quantum yields  
20 ranging from  $9.3 \cdot 10^{-8}$  to  $6.4 \cdot 10^{-7}$  in the Sargasso Sea for Weiss et al., 1995a and Zepp et al.,  
21 1994, respectively). The quantum yields depend both on the location and the season of the  
22 measurement, especially because CDOM quality and its absorption coefficient might vary  
23 through time (Kettle et al., 2002; Weiss, 1995b; Cutter et al., 2004). To compensate for part of  
24 this natural variability, Uher et al. (1997) normalized the measured AQY by the absorption  
25 coefficient of CDOM available for the reaction at the same location. Therefore, the new  
26 relation, implemented in NEMO-PISCES, is the following:

$$27 \quad P = a_{350} \, UV \frac{p}{a_{350}} = k \, a_{350} \, UV \quad (7b)$$

28 where  $P$  is the OCS photo-production rate ( $\text{pmol m}^{-3} \text{s}^{-1}$ ),  $UV$  is the incident irradiance  
29 integrated from 295 to 385nm ( $\text{W m}^{-2}$ ). The  $k$  coefficient is retrieved from the normalization  
30 of measured photoproduction constants to measured CDOM absorption coefficient values at  
31 350 nm. For offshore waters (the majority of globe waters),  $k$  was found, in Uher et al. (1997)  
32 study, to be close to a value of  $2.1 \text{ fmol L}^{-1} \text{ s}^{-1} \text{W}^{-1} \text{m}^3$ . Note that the  $k$  coefficient deduced  
33 from inshore water samples was found to be  $2.8 \text{ fmol L}^{-1} \text{ s}^{-1} \text{W}^{-1} \text{m}^3$  on average. The smaller



1 difference between the two k values justified the choice to use this normalized expression  
2 rather than Eq. 7a which showed more sample-dependence.

### 3 **2.2.4 Parameterization of OCS dark-production rates**

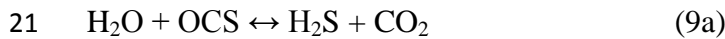
4 Measurements of large OCS concentrations well below the photic zones have proven that  
5 OCS can be produced when no light is available. The so-called dark-production pathway was  
6 shown to largely depend on available organic matter. The pool of organic matter is quantified  
7 by the  $a_{350}$  parameter, following Para et al. (2010), as explained in Section 2.2.2. Microbial  
8 activities are suggested as main precursors for the OCS dark-production pathway, but their  
9 exact nature and the mechanisms underlying this process are poorly known. Von Hobe et al.  
10 (2001, 2003) calculated dark-production rates assuming that after dawn OCS concentrations  
11 were reaching a steady-state when dark-production was compensating for the parallel  
12 hydrolysis. Equation 8 was established using measurements from a campaign in the Sargasso  
13 Sea and hydrolysis rates were calculated following the Elliott et al. formulation (1989).  
14 The formulation from Von Hobe et al. (2001) relating OCS dark-production rates to the  
15 CDOM absorption coefficient was implemented in NEMO-PISCES following:

$$16 \quad Q = a_{350} e^{(55.8 - \frac{16200}{T})} \quad (\text{T in K}) \quad (8)$$

17 where Q is the dark-production rate in  $\text{pmol m}^{-3} \text{s}^{-1}$ , and  $a_{350}$  is the CDOM absorption  
18 coefficient which is used here to describe the CDOM/organic matter concentration.

### 19 **2.2.5 Hydrolysis of OCS**

20 OCS is chemically removed in seawater through reaction with  $\text{H}_2\text{O}$  and  $\text{OH}^-$ :



23 OCS hydrolysis rate measurements were done in the dark, using filtered water, therefore  
24 cancelling the potential impact of parallel dark-production. Reactions 9a and 9b are actually  
25 composites of complex mechanisms involving several intermediates, and concentrations that  
26 have been used to calculate hydrolysis rates are much larger than observed in seawater, which  
27 may lead to some errors.

28 We performed sensitivity tests in NEMO-PISCES by using two different hydrolysis  
29 parameterizations to study the impact of the choice of the hydrolysis constant formulation.  
30 Both Kamyshny et al. (2003) and Elliott et al. (1989) relate the value of OCS hydrolysis  
31 constant to the marine water pH and its temperature, following respectively:

$$32 \quad k_{hydr\_Elliott} = e^{(24.3 - \frac{10450}{T})} + \frac{k_w}{[H^+]} e^{(22.8 - \frac{6040}{T})} \quad (\text{T in K}) \quad (10a)$$

$$k_{hydr\_Kamyshny} = 4.19E^{-12} e^{\left(\frac{-12110}{T}\right)} + \frac{k_w}{[OH^-]} 1.41E^{18} e^{\left(\frac{-11580}{T}\right)} \quad (T \text{ in K}) \quad (10b)$$

2

3 With  $k_w$  the ion product of marine water,  $[OH^-]$  and  $[H^+]$  the  $OH^-$  and  $H^+$  activities.

4 Both hydrolysis constant rates, as function of temperature, are represented in the case of  
5  $pH=8.2$  in Fig. 2.

## 6 **2.2.6 OCS sea-to-air fluxes**

7 OCS exchange between the ocean and the atmosphere can be described in an analogous way  
8 to Fick's diffusion law. The sea-air OCS flux depends on the OCS concentration in sea water  
9 and the partial pressure of OCS in air:

$$F_{OCS} = k_{water} \left( [OCS]_{aq} - \frac{[OCS]_{atm}}{H} \right) \quad (11)$$

11 where  $F_{OCS}$  is the sea-air flux ( $\text{pmol m}^{-2} \text{s}^{-1}$ ),  $[OCS]_{aq}$  and  $[OCS]_{atm}$  are the OCS concentration  
12 at sea surface and in the atmosphere respectively (in  $\text{pmol m}^{-3}$ ). The atmospheric OCS  
13 concentration  $[OCS]_{atm}$  over sea surface was constantly imposed when running NEMO-  
14 PISCES, assuming an atmospheric mixing ratio of 500 ppt. Through  $H$ , the Henry's law  
15 constant, the sea-air OCS flux also depends on the air temperature, and was implemented in  
16 NEMO-PISCES following the expression established by Johnson et al. (1986):

$$H = e^{\left(\frac{12722 - \frac{3496}{T}}{T}\right)} \quad (T, \text{ air temperature in K}) \quad (12)$$

18  $k_{water}$  is the piston velocity (in  $\text{m.s}^{-1}$ ) for OCS. The coefficient is deduced from the Schmidt  
19 number of OCS and depends on surface wind speed, and is calculated with the relation of  
20 Wanninkhof (1992):

$$k_{water} = [0.3u^2 + 2.5 * (0.5246 + 0.016256T + 0.00049946T^2)] * \sqrt{\frac{660}{S_{OCS}}} \quad (T \text{ air} \\ \text{temperature in } ^\circ\text{C}) \quad (13)$$

23 Where  $u$  is the wind speed (in  $\text{m.s}^{-1}$ ).

24 Note that Kettle et al. (2002) used similar parameterizations for the sea-surface exchange  
25 coefficient and the same relation from Wanninkhof et al. (1992) to model the global OCS flux  
26 at sea surface to the one presented in this work.

1 The Schmidt number for OCS,  $S_{ocs}$ , dimensionless, was implemented in NEMO-PISCES  
 2 following the suggestion by Ulshöfer (1995) to deduce it from kinetic viscosity ( $\nu$ ) and  
 3 diffusion coefficient (D) (both in  $\text{m}^2 \cdot \text{s}^{-1}$ ), respectively derived from:

$$4 \quad S_{ocs} = \frac{\nu}{D} \quad (14)$$

5 with:

$$6 \quad \nu = (1.792747 - 5.126103E^{-2}T + 5.918645E^{-4}T^2) * 1E^{-6} \quad (T, \text{air temperature in } ^\circ\text{C})$$

7 (15)

$$8 \quad D = \left(10^{\left(\frac{-1010}{T}\right) - 1.3246}\right) * 1E^{-4} \quad (T, \text{air temperature in K}) \quad (16)$$

### 9 **2.3 An independent appraisal of photo-production rates**

10 Independently from NEMO-PISCES, the photochemical model of Fichot and Miller (2010)  
 11 was used to calculate monthly climatologies of depth-integrated photo-production rates of  
 12 OCS in the global ocean. Briefly, the photochemical model used three components to  
 13 calculate depth-resolved photochemical rates in the global ocean: 1) a radiative transfer model  
 14 for the determination of cloud-corrected UV-visible (290-490 nm) downward scalar  
 15 irradiance, 2) the SeaUV algorithm (Fichot et al., 2008), used to calculate the spectral diffuse  
 16 attenuation coefficient of UV and CDOM absorption coefficient (290-490 nm) from satellite  
 17 ocean color data, and 3) published AQY for the photochemical process of interest. To  
 18 describe the observed variability in AQY, both mean values from Weiss et al. (1995a) (open  
 19 ocean) and that of Zepp et al. (1994) (coastal ocean) were used in this study. Small  
 20 modifications to the original photochemical model were also made, including the use of  
 21 MODIS *Aqua* ocean color data (instead of SeaWiFS), and the use of a 2 nm spectral  
 22 resolution (instead of 5 nm). The photoproduction rates are later compared to the NEMO-  
 23 PISCES simulated rates and to other seawater measurements (e.g. Cutter et al., 2004).

24

### 25 **3 Results**

26 The absorption coefficient of CDOM at 350 nm ( $a_{350}$ ) increased monotonically with  
 27 chlorophyll concentration for low chlorophyll contents. The different  $a_{350}$ -chlorophyll  
 28 relations used in this paper led to large differences in  $a_{350}$  estimates, especially at high  
 29 chlorophyll levels in seawater (Fig. 3). Estimates of  $a_{350}$  obtained with the relation based on  
 30 MODIS *aqua* ocean color, that we proposed (Eq.(6)), provided values two to three times

1 larger than  $a_{350}$  values obtained with the relation from Preiswerk et al. (2000). Since both  
2 photo- and dark-production are modeled as linear functions of  $a_{350}$ ,  
3 underestimating/overestimating chlorophyll concentrations directly lead to  
4 underestimated/overestimated OCS production. Therefore, the evaluation of chlorophyll  
5 concentration is of capital importance in the present work.

### 6 **3.1 Evaluation of chlorophyll concentration at the global scale**

7 Modeled annual mean surface chlorophyll concentrations from NEMO-PISCES compared  
8 relatively well with SeaWiFS chlorophyll observations (Fig.4). The model correctly  
9 represented main spatial patterns with for instance high latitudes showing higher annual mean  
10 chlorophyll concentrations and a stronger seasonal cycle. Observed mid- and high-latitude  
11 chlorophyll levels showed values three to four times larger than chlorophyll levels in tropical  
12 regions, which was also well captured with NEMO-PISCES. However, the model generally  
13 underestimated the chlorophyll concentration in the most oligotrophic subtropical zones of the  
14 global ocean.

### 15 **3.2 Evaluation of the depth-distribution of $a_{350}$ and OCS concentrations**

16 In order to provide an evaluation of modeled vertical distributions of OCS concentrations, in  
17 this subsection we present vertical monthly mean profiles of  $a_{350}$  and OCS concentration from  
18 1D simulation runs with NEMO-PISCES. Wherever possible, we compared these simulated  
19 profiles with relevant in situ measurements. A majority of them were taken in the site of  
20 BATS (31°N, 64°W). In situ measurements for OCS concentrations remain scarce at this  
21 point. Evaluations of the contribution of each individual OCS formation and destruction  
22 processes are even scarcer. Therefore, the cruise measurements around the BATS site from  
23 Cutter et al. (2004) are often used as a reference.

#### 24 **3.2.1 Vertical profiles for $a_{350}$**

25 Our MODIS-*Aqua* based extrapolation (Eq. (6)) resulted in the highest values of simulated  
26  $a_{350}$  (up to  $0.15 \text{ m}^{-1}$ , both in January and in August), while the parameterization from  
27 Preiswerk et al.(2000) resulted in  $a_{350}$  values that were about half as much (Fig. 5), consistent  
28 with the difference in the respective  $a_{350}$ -chlorophyll formulations (Fig. 3). Values for  $a_{350}$   
29 deduced from Morel and Gentili (2009) (Eq. (2)) gave an intermediary result. The pronounced  
30 August maximum around 80 m depth (Fig. 5, B) reflected a chlorophyll content maximum at  
31 this depth ( $a_{350}$  is monotonically increasing for low levels of chlorophyll). In contrast, low  $a_{350}$

1 values near the surface translated to a local minimum in the chlorophyll content. Note also the  
2 abrupt decrease of chlorophyll concentrations, and therefore the decreasing  $a_{350}$ , for depths  
3 below 80 m in August. In January the mixed layer was 120m-thick in NEMO-PISCES at the  
4 BATS site (Fig. 5, A). Chlorophyll content (thus  $a_{350}$ ) remained high and constant over the  
5 first 120 m of the ocean before an abrupt decrease in the pycnocline. For both January and  
6 August, chlorophyll concentrations and  $a_{350}$  values became negligible below 200m, with the  
7 exception of  $a_{350}$  calculated with the relation proposed in this work.

8

### 9 **3.2.2 Vertical OCS concentration profiles**

10 Differences in  $a_{350}$  estimations using the relations in Eq. (2) to Eq. (6) led to 3-fold difference  
11 between the most extreme near-surface OCS maximum concentrations simulated by NEMO-  
12 PISCES (from 100 to 300  $\text{pmol L}^{-1}$  in August and from 30 to 85  $\text{pmol L}^{-1}$  in January). In the  
13 photic zone (the first 30 m below the surface, as implemented in NEMO-PISCES), August  
14 subsurface OCS concentrations (Fig. 5, D) were clearly driven by the photo-production  
15 (vertical profile of photo-production not shown here). Where the influence of UV-light  
16 irradiance is smaller or negligible (below 30 m in August or in the entire water column in  
17 January), OCS concentration profiles are driven by the predominant dark-production (vertical  
18 profile of the dark-production contribution not shown here). Therefore, in these layers, OCS  
19 concentrations mostly followed the chlorophyll content profiles. Thus, OCS concentration  
20 profiles simulated with NEMO-PISCES in January showed a drop below the mixed layer  
21 (below 120m), and became negligible below 200m. In August, the highest concentrations  
22 were found at the surface. A second peak of OCS levels was found around 80 m depth, where  
23 chlorophyll content peaks. Deeper, the OCS concentrations decreased, down to negligible  
24 values below 200m.

25 OCS concentrations simulated with NEMO-PISCES showed very large values in the few first  
26 meters under the surface, averaging 70, 90 or even 270  $\text{pmol L}^{-1}$  in August at BATS site,  
27 depending on the  $a_{350}$ -chlorophyll relation used. Some OCS levels measured with buoys  
28 during a field campaign in August 1999 at BATS peaked at 150  $\text{pmol L}^{-1}$  in the first 3 meters  
29 (Cutter et al. 2004), showing a potential to reach such high values. When using the  $a_{350}$   
30 formulas derived from the studies of Morel and Gentili (2009) or Preiswerk (2000), the  
31 simulated vertical profiles of OCS concentrations in the Sargasso Sea in August (Fig. 5D) fall  
32 into the range of measured OCS concentrations reported by Cutter et al. (2004). This is

1 however not the case when using the  $a_{350}$  based on MODIS-aqua data which lead to the  
2 highest simulated OCS concentrations (270 pmol L<sup>-1</sup> at the sea surface) and seem to  
3 overestimate the natural variability of the OCS concentrations, as measured in these waters.

4 The lower OCS concentrations in deeper layers reflected the quick removal of OCS by  
5 hydrolysis in the model (vertical profile of the hydrolysis contribution not shown here). This  
6 behavior fit well with the estimated short lifetime of the OCS molecule in marine waters,  
7 ranging between 4 and 13.4 hours, according to the models of Elliot et al. (1989) and  
8 Radford-Knoery and Cutter (1993), respectively.

9

### 10 **3.3 Spatial and seasonal variability of OCS production and removal processes**

#### 11 **3.3.1 Surface $a_{350}$ patterns**

12 Absorption coefficients of CDOM at 350 nm ( $a_{350}$ ) simulated using NEMO-PISCES were  
13 evaluated for the different formulations of  $a_{350}$  against the annual climatology of  $a_{350}$  derived  
14 from MODIS *Aqua* ocean color as in Fichot and Miller (2010). The MODIS *Aqua*-derived  
15  $a_{350}$  (Fig. 6, panel A) showed minimal values in the subtropical gyres, and maximum values in  
16 coastal regions and at high latitudes (higher than 45°N and 45°S). Note that the MODIS *Aqua*  
17 derived values should not be considered as direct observations but only as an independent  
18 estimate relying on a generic relation (i.e., a statistical model).

19 Regions where  $a_{350}$  was not accurately modeled also suffered from biases in simulated  
20 chlorophyll values. Therefore the highest  $a_{350}$  values observed near the coasts were not  
21 represented in NEMO-PISCES due to its limited spatial resolution. Additionally, the  
22 simulated chlorophyll maps (thus those of  $a_{350}$  as well) showed a higher contrast between low  
23 and high latitudes than the SeaWiFS derived observations (Fig. 4). In tropical regions (30°S-  
24 30°N), especially in the Atlantic Ocean, the Indian Ocean and in the Western Pacific Warm  
25 Pool, chlorophyll levels simulated by NEMO-PISCES were underestimated by a factor of two  
26 compared to the SeaWiFS chlorophyll observations (Fig. 4). As these are regions of warm  
27 ocean waters favorable to OCS dark-production, the consequence might be an  
28 underestimation of OCS production in these regions. In regions showing low chlorophyll  
29 concentrations, this underestimation translates to an approximately 30% underestimation of  
30 the  $a_{350}$  value (depending on the  $a_{350}$  formulation used), which directly translates to an  
31 equivalent underestimation of OCS dark- and photo-production, since both parameterization  
32 linearly depend on  $a_{350}$ .

1 Finally, NEMO-PISCES-simulated chlorophyll levels at mid- and high-latitudes were similar  
2 for northern and southern oceans, with average values around  $0.5 \text{ mg m}^{-3}$ . However,  
3 chlorophyll concentrations deduced from satellite observations showed average mid- and  
4 high-latitude values around  $0.2 \text{ mg m}^{-3}$  in the Southern Hemisphere and  $0.5$  to  $1 \text{ mg m}^{-3}$  in the  
5 Northern Hemisphere. Thus, the NEMO-PISCES model overestimated the chlorophyll  
6 concentrations by a factor of 2 over most of the mid- and high-latitudes of the Southern  
7 Hemisphere - especially in the Pacific Ocean and south of Australia (Fig. 4). Therefore, our  
8 modeled OCS production in the Southern Hemisphere is likely overestimated.

9 The different  $a_{350}$ -chlorophyll relations used in the present work (Eq. (2), Eq. (3) and Eq.(6))  
10 led to simulated values of  $a_{350}$  differing by as much as a factor of three. The CDOM  
11 absorption coefficient values obtained with the formulations of Preiswerk et al. (2000) and  
12 Morel and Gentili (2009) were similar to the MODIS-derived estimates for low- and mid-  
13 latitudes (below  $60^\circ\text{S}$  and  $60^\circ\text{N}$ ), but largely underestimated at high latitudes in the Northern  
14 Hemisphere, with values two to three times smaller than the MODIS-derived estimates (Fig.  
15 6). Conversely, the formulation presented in this work (Eq. (6)) correctly reproduced the  
16 observed levels of  $a_{350}$  in the northern high latitudes, but clearly overestimated the values for  
17 CDOM absorption coefficient at low latitudes and in the Southern Hemisphere: simulated  $a_{350}$   
18 values in some subtropical oligotrophic regions reached values three to four times higher than  
19 the MODIS derived values.

### 20 **3.3.2 Photo-production rates**

21 In the present study, the  $a_{350}$ -dependent NEMO-PISCES model and the AQY dependent  
22 photochemical model from Fichot and Miller (2010) were used to provide two independent  
23 estimates of OCS photo-production rates. Sensitivity tests were performed on the annual  
24 global OCS photo-production over the entire water column (from the sea surface to the ocean  
25 floor). Both models were run with different formulations of  $a_{350}$  (NEMO-PISCES model) or  
26 using different AQY (Fichot and Miller photochemical model) from the literature.

27 The AQY estimates used were collected in open ocean environments (Weiss et al., 1995a) and  
28 coastal environments (Zepp et al., 1994), respectively. Large uncertainties around AQY  
29 estimations depending on the measurement location led to large differences in the estimates of  
30 global OCS photo-production. Global OCS photo-production modeled with Fichot and  
31 Miller's model (2010) thus ranged from  $876$  to  $5,500 \text{ GgS yr}^{-1}$  (Table 1). Extremely high  
32 AQY values have been measured on the continental shelf (Cutter et al., 2004), but were not  
33 considered appropriate to represent the global average ocean. Using this last value would have

1 led to 37,700 GgS yr<sup>-1</sup> of OCS global photoproduction, far above observed photo-production  
2 levels and other model estimates.

3 Both the photochemical model from Fichot and Miller (2010) and the NEMO-PISCES model  
4 led to similar spatial distributions of OCS photo-production (Fig. 7). Indeed, subtropical  
5 regions are the major contributors in terms of yearly total photo-production of OCS, because  
6 the photo-production rates were roughly constant through the entire year, whichever model  
7 was used. However, the highest monthly photo-production rates were found in mid-latitude  
8 regions (40-60°N and 40-60°S) during the period of maximum irradiance, with rates twice as  
9 large as the nearly constant rates obtained in tropical regions, as can be seen in the time-  
10 latitude diagram in Fig. 8 (panel A). Depending on the value of the driving parameter for the 2  
11 models used (AQY or  $a_{350}$ , respectively), large uncertainties existed over the total quantities  
12 of OCS photo-produced. Global photo-production of OCS for the NEMO-PISCES model and  
13 the photochemical model from Fichot and Miller (2010) are compared in Table 1. When using  
14 the  $a_{350}$ -based model NEMO-PISCES, the range of the global OCS photo-production was  
15 reduced but still large, with estimates between 1,390 and 4,540 GgS yr<sup>-1</sup>, depending on which  
16 formulation was chosen to calculate  $a_{350}$ . These values were in rather good agreement with the  
17 range obtained with the AQY-based photochemical model from Fichot and Miller (2010).

18 The photochemical model from Fichot and Miller and NEMO-PISCES showed lower OCS  
19 photo-production rates than in situ measurements, irrespective of the  $a_{350}$  formulation. For  
20 instance, Cutter et al. (2004) estimated August photo-production rates up to 10 or 15 pmol L<sup>-1</sup>  
21 h<sup>-1</sup> in the Sargasso Sea, which is above the values of 4 to 9 pmol L<sup>-1</sup> h<sup>-1</sup> obtained by running  
22 the NEMO-PISCES model at the same location (with implemented Eq. (3) and Eq. (6)  
23 respectively) (Fig. 7).

### 24 **3.3.3 Dark-production rates**

25 Dark-production is a linear function of  $a_{350}$  (Eq. (8)). However, temperature is the main driver  
26 of global OCS dark-production as simulated by NEMO-PISCES. The time-latitude  
27 representation of dark-production rates (Fig. 8, panel B) showed that the maximum values  
28 were located at low latitudes, in warm marine waters, despite the fact that these regions  
29 correspond to the lowest  $a_{350}$  values (Fig. 6). The dark-production rates in these regions  
30 remained relatively constant throughout the year. On the contrary, chlorophyll-rich waters at  
31 higher latitudes, leading to higher  $a_{350}$  values (Fig. 6) corresponded to colder marine waters  
32 and thus limited dark-production rates (due to the temperature dependency in Eq. (8)).



1 Measurements from Von Hobe et al. (2001) at the BATS site showed dark-production rates of  
2 1 to 1.5 pmol L<sup>-1</sup> h<sup>-1</sup>. NEMO-PISCES results showed a very good agreement with this data,  
3 with rates of 0.8 pmol L<sup>-1</sup> h<sup>-1</sup> in August at BATS (not shown). In the study of Cutter et al.  
4 (2004), calculated dark-production rates reached 4 pmol L<sup>-1</sup> h<sup>-1</sup> in August, significantly above  
5 the simulated range by NEMO-PISCES. Von Hobe et al. (2001) estimated that dark-  
6 production produces around 50% of OCS at these low latitudes. In the NEMO-PISCES  
7 model, dark-production only represented 34% of the OCS produced at low latitudes, and 66%  
8 of OCS is photo-produced.

### 9 **3.3.4 Hydrolysis rates**

10 Figure 2 presents the hydrolysis reaction constant as a function of temperature for a given pH,  
11 as given by the Kamyshny et al. (2003) and Elliott et al. (1989) formulations. Both  
12 formulations relate the OCS hydrolysis to the OCS concentration and to the seawater pH (Eq.  
13 (10a) and Eq. (10b)). At a given pH, the difference between the two formulations was leading  
14 to a 50% difference in the hydrolysis constant for seawater temperatures above 12°C (Fig. 2).  
15 A comparison between time-latitude maps of the hydrolysis rate (Fig. 8, panel C) and the  
16 OCS concentration (in Fig A1) suggests that OCS hydrolysis rates in NEMO-PISCES are  
17 largely driven by OCS concentrations. These spatio-temporal variation patterns only slightly  
18 differ around the equator, where marine waters are somewhat less alkaline, which leads to a  
19 limitation of the OCS hydrolysis rate through pH influence. Simulations run with two  
20 different hydrolysis parameterizations (based on Eq. (10a) or Eq. (10b)) provide global OCS  
21 emissions diverging by a factor of 2.5 (see Fig. 9).

### 22 **3.3.5 Evaluation of surface concentration patterns**

23 Maps of annual mean surface OCS concentration patterns at sea surface simulated with  
24 NEMO-PISCES are presented on Fig. 10 (right column). NEMO-PISCES simulations  
25 produced maximum annual mean OCS levels in equatorial and sub-tropical regions, where  
26 dark-production was maximal and photo-production was constantly active. In low latitude  
27 marine waters, OCS concentrations remained nearly constant throughout the year (Fig A1 and  
28 Fig. 10). However, the model showed a strong seasonal variability of OCS concentrations for  
29 mid- and high latitudes, with roughly a factor 10 difference between maximal and minimal  
30 OCS concentration levels reached throughout the year. These spatial distributions and the  
31 intra-annual variation amplitudes were relatively independent of the formulation used in  
32 NEMO-PISCES to calculate  $a_{350}$ .

1 Modeled OCS concentrations were evaluated against observational data available in the  
2 literature. OCS concentrations measured near European shores and estuarine regions over the  
3 year, showed large spatial and temporal variability (Uher, 2006). The few measured OCS  
4 concentrations in estuarine regions were close to 250 pmol L<sup>-1</sup> in winter and 430 pmol L<sup>-1</sup> in  
5 summer, while smaller values were measured near shores, from 40 pmol L<sup>-1</sup> in winter to 100  
6 pmol L<sup>-1</sup> in summer. Von Hobe et al. (2003) also measured summer OCS surface maximum  
7 levels of 120 pmol L<sup>-1</sup>, in an upwelling region near the Portuguese coast. When using the  
8 MODIS-*Aqua*-based  $a_{350}$  formulation (Eq. (6)) which gives the best representation of  $a_{350}$  in  
9 the region (Fig.6), simulated OCS concentrations near shores only reached values from 30  
10 pmol L<sup>-1</sup> in winter to 100 pmol L<sup>-1</sup> in summer (Fig. 10). NEMO-PISCES matches correctly  
11 the seasonal amplitude of OCS concentrations measured in these areas and represents quite  
12 accurately the absolute values measured near the shores. However, as expected, the lack of  
13 resolution of the model translates into an under-estimation of the estuarine concentrations.

14 As shown in the comparison done in the study of von Hobe et al. (2003), the reproduction of  
15 the OCS depth profiles by their models was generally less accurate than that of surface data  
16 because the models were tuned to fit the surface concentrations. In our study, the model was  
17 not tuned to fit surface or depth concentrations. As NEMO-PISCES provides gridded monthly  
18 mean concentrations of OCS on the entire water column, monthly mean concentrations of  
19 OCS data series should, ideally, be used to evaluate the global simulations.

20 Unfortunately, a global database of sea surface OCS measurements and a procedure to  
21 calculate sea surface OCS as a function of latitude, longitude, and month are not available in  
22 the literature as, for example, for DMS (e.g. Kettle et al., 1999; Lana et al, 2011). The  
23 assemblage of a global OCS database was not achievable in the framework of this project.  
24 The evaluation of the modeled oceanic OCS concentrations that had been carried out is not  
25 fully satisfactory because we implicitly accepted to compare modeled monthly mean  
26 concentrations and discrete measurements.

27 With these caveats in mind, 150 OCS measurements classified according to location, date and  
28 depth were gathered from the literature (Weiss et al., 1995a ; Ulshofer et al., 1996 ; Cutter et  
29 al., 2004 ; Von Hobe et al., 2001 and 2003) and compared with the outputs from the model  
30 run with its “standard” parameterization, as described in the discussion section. The results  
31 are displayed in Fig. A2 and show that the outputs of the model generally overestimate the  
32 measured concentrations by a factor of two to four at the sea surface (first 10m, A), especially  
33 at sites where low concentrations were measured. In seawaters with high OCS concentration

1 measurements (higher than  $100 \text{ pmol L}^{-1}$ ), the corresponding simulated concentrations were  
2 generally underestimated, up to a factor of two. A better agreement between modeled and  
3 observed concentrations is found with the subsurface data (below 10m, B).  
4 This model-data comparison suggests that simulated OCS concentrations might be  
5 overestimated in a significant way in surface waters, which might lead to an overestimation of  
6 the simulated OCS outgassing fluxes (up to factors of two to four). However, the limited  
7 spatial (many measurements were done around  $40^\circ\text{N}$ ) and temporal (many measurements in  
8 July and August) distribution of the measurements severely reduced the possibility for an  
9 exhaustive model validation and for the identification of concentration biases in the model.  
10 Furthermore, a large range of concentrations were measured even for sites close in latitude  
11 and/or for measurements realized around the same period of the year. Finally, this over-  
12 estimation might also compensate for the under-estimation in the OCS production in shallow  
13 water, since the model is lacking an exhaustive representation of the estuarines regions.  
14 The formulation used to calculate  $a_{350}$  values did not affect the global spatial distribution of  
15 OCS concentrations, but it largely influenced the absolute value of the simulated OCS  
16 concentrations. For instance, maximal OCS concentrations in tropical sub-surface waters were  
17 estimated close to  $300 \text{ pmol L}^{-1}$  with the MODIS-*Aqua*-based  $a_{350}$  formulation (Eq. (6)), while  
18 Morel and Gentili (2009) (Preiswerk et al., 2000)-based estimates only reached one half (one  
19 third, respectively) of these modeled maximal concentrations (Fig. 10). Note that the  
20 formulation of Morel and Gentili (2009) led to results that were in better agreement with the  
21 campaign measurements described in section 3.2.2 (Cutter et al, 2004; von Hobe et al., 2001).

22

#### 23 **4 Discussion**

24 The limited number of studies which have attempted to quantify OCS production and removal  
25 processes individually have yielded widely differing results. Several parameterizations for  
26 each process have been proposed and each parameterization remains poorly constrained. In  
27 this section we present our “best guess” formulations for the individual OCS-related processes  
28 in the NEMO-PISCES model.

29 Measurement campaigns used to determine dark-production functions are particularly scarce.  
30 The dark-production parameterization that we used is related to the CDOM absorption  
31 coefficient at 350 nm, as a parameterization of the link with organic matter content and  
32 biological activity in marine environments. However, there is no rationale for dark-production

1 to be dependent of colored organic matter content (CDOM, chlorophyll) since this process  
2 occurs at times when no light is available.

3 In a rare example of observation-based dark-production parameterization effort, von Hobe et  
4 al. (2003) used an experimental setup that allows them to equate the OCS dark-production  
5 rate to the hydrolysis rate, and thus expressed the first as a function of a measurement of the  
6 latter. In their estimate of the hydrolysis rate, von Hobe et al. (2003) use the Elliott et al.  
7 (1989) formulation for the OCS hydrolysis constant. Thus, our use of the von Hobe et al.  
8 (2003) dark-production parameterization is consistent with the choice of the Elliott et al.  
9 (1989) parameterization for OCS hydrolysis.

10 As previously described, simulated  $a_{350}$  values can be far from the observed values in warm  
11 water regions depending on the  $a_{350}$  formulation used (Fig. 6). This potentially leads to the  
12 largest errors in the dark-production rate estimates. In this context, we have found the Morel  
13 and Gentili (2009)  $a_{350}$  parameterization to perform best when evaluated against  $a_{350}$  values  
14 derived from MODIS-*Aqua* data at low latitudes, as well as at high latitudes in the Southern  
15 Hemisphere (section 3.3.1). This formulation may, however, lead to an underestimation of  
16  $a_{350}$  at high latitudes in Northern Hemisphere.

17 We have chosen the Uher et al. (1997) formulation for photoproduction associated with the  
18 Morel and Gentili parameterization for  $a_{350}$  (Eq. (2)) and the Elliott formulation for the  
19 hydrolysis constant as the standard parameterizations for OCS processes in NEMO-PISCES,  
20 based on the arguments above. Time-latitude diagrams for photo- and dark-production,  
21 hydrolysis and surface OCS fluxes using these parameterizations are represented in Fig. 8.  
22 The time-latitude diagram representing the surface layer OCS concentration with the same  
23 settings is shown in Fig A1.

24 The standard run of NEMO-PISCES suggests most OCS is produced photochemically. Even  
25 at low latitudes, where warm water regions favor dark-production of OCS, photo-production  
26 represents 66% of OCS production pathway (Fig. 8). In this simulation, low latitudes are the  
27 only regions where dark-production rates compensate for hydrolysis removal of OCS. The  
28 highest annual mean OCS concentrations modeled using best guess parameterizations range  
29 between 100 and 200 pmol L<sup>-1</sup> and are encountered around the equator, especially in Central  
30 and Eastern Pacific Ocean. At mid and high latitudes, simulated annual mean OCS  
31 concentrations are included between 10 and 60 pmol L<sup>-1</sup>. These regions show higher seasonal  
32 amplitude in OCS concentrations, especially around 60°N and 40°S, where periods of

1 irradiance maxima (resp. minima) lead to simulated OCS concentrations of 150 pmol L<sup>-1</sup>  
2 (resp. 10 pmol L<sup>-1</sup>). In these regions, simulated concentrations are largely consistent with in  
3 situ measurements from Cutter et al. (2004) and Von Hobe et al. (2003).

4 Surface OCS concentrations simulated by NEMO-PISCES are the main driver of the model's  
5 sea-air OCS fluxes (Fig. 8, panel D and Fig A1). The regions with the highest sea surface  
6 OCS concentrations (tropics and mid-latitudes during maximal irradiance seasons) are the  
7 regions emitting the largest quantities of OCS. Multiple measurement campaigns (Rasmussen,  
8 Khalil and Hoyt, 1982; Ferek and Andreae, 1983; Uher, 2006) have shown that coastal  
9 environments can have OCS concentrations 5 to 10 times higher than those measured at the  
10 surface of open ocean waters in oligotrophic regions. As shown in Fig.6, MODIS-derived a<sub>350</sub>  
11 reach maximal values along shores but the NEMO-PISCES model does not represent these  
12 localized maxima due to the poor model resolution in these regions. These narrow areas have  
13 an important potential in OCS production and show under-estimated OCS concentrations in  
14 NEMO-PISCES.

15 Air-sea exchange of OCS is also enhanced by warm surface waters and strong winds (Eq.  
16 (11)). Both variables have a noticeable impact on the simulated OCS surface fluxes,  
17 especially at low latitudes. In fact, NEMO-PISCES simulations show the highest OCS  
18 emissions around the equator even if some mid- and high-latitude oceanic regions show  
19 higher OCS sea surface concentrations for some periods of the year: OCS outgassing rates in  
20 July along the Equator are twice as important as outgassing taking place in Northern mid-  
21 latitudes in the same period (Fig. 8, panel D), despite the mid-latitudes showing surface OCS  
22 concentrations 60% higher than those simulated around the Equator.

23 We have investigated the sensitivity of the sea-air fluxes to the parameterizations of OCS  
24 production and removal processes. Global and regional annual sea-air OCS fluxes obtained in  
25 these tests are summarized in Fig. 9. Simulated fluxes by Kettle et al. (2002) are also  
26 represented on the figure 9 (black line) for comparison. While the different parameterization  
27 choices lead to a large spread in the simulated OCS fluxes towards the atmosphere, NEMO-  
28 PISCES consistently produces higher estimates of the global sea-air OCS fluxes than the ones  
29 previously estimated by Kettle et al. (2002). Total emitted OCS simulated using the “best  
30 guess” parameterization of NEMO-PISCES reaches 813 GgS yr<sup>-1</sup>, far above the modeled  
31 direct source of 40 GgS yr<sup>-1</sup> from Kettle et al. (2002) and consistent with the revised global  
32 oceanic flux based on atmospheric measurements and a model for leaf uptake, proposed by

1 Berry et al. (736 GgS yr<sup>-1</sup>). Extrapolations of measurements carried out in the Mediterranean  
2 sea and the Indian ocean by Mihalopoulos et al. (1992) led to an independent estimate of 213  
3 GgS yr<sup>-1</sup>, markedly lower than the mean annual global flux simulated with NEMO-PISCES.  
4 Kettle et al. (2002) described the global direct exchange of OCS between the ocean and the  
5 atmosphere as highly uncertain, and pointed out the fact that in some of their simulations,  
6 some regions of the ocean behaved like sinks of atmospheric OCS at certain periods of the  
7 year. Some regions at extreme high latitudes also act like a sink of atmospheric OCS in  
8 NEMO-PISCES for certain periods of the year (Fig. 8, panel D).

9- The different parameterizations available for the different processes presented in this paper  
10 lead to different global flux estimates, ranging from 573 GgS yr<sup>-1</sup> (when using the CDOM  
11 absorption coefficient values obtained with the formulations of Preiswerk et al. (2000) and the  
12 higher values of the Elliot-based hydrolysis constant) to 3997 GgS yr<sup>-1</sup> (when using the  
13 MODIS-derived  $a_{350}$  and the lower values of the Kamyshny-based hydrolysis constant). Our  
14 “best-guess” parameterization of NEMO-PISCES shows the best agreement with the in situ  
15 evaluation of the individual processes, and stands in the lower part of the range of OCS direct  
16 annual emissions by ocean at a global scale.

17- Changing the parameterization also changes the seasonal amplitude of the simulated OCS  
18 flux by up to a factor five for Northern and Southern Hemisphere oceans but no significant  
19 change is noticeable on the seasonal amplitude of OCS fluxes in the tropical region.

20 Recent efforts to constrain global OCS fluxes have led to a growing number of measurements  
21 and consequent revisions of soil and vegetation uptake estimates. Multiple recent studies have  
22 suggested that soil and vegetation uptakes were underestimated in the new assessments of the  
23 global OCS cycle and have suggested a global sink for both of up to 1000 GgS yr<sup>-1</sup> (Berry et  
24 al., 2013; Suntharalingam et al., 2008), much larger than the estimates of approximately 300  
25 GgS yr<sup>-1</sup> by Kettle et al. (2002). Knowing that atmospheric OCS levels show no trend over the  
26 last two decades (Montzka et al., 2007), the global cycle of OCS is expected to be balanced  
27 on a global scale. In order to compensate re-estimated sinks based on a mechanistic  
28 description of leaf OCS uptake (using SIB3 land surface model), Berry et al. (2013) have  
29 suggested that the ocean provides the missing source. Using a simple inversion approach to  
30 optimize the oceanic missing source, given known land natural and anthropogenic fluxes, the  
31 authors evaluated that the ocean should emit 736 GgS yr<sup>-1</sup>. Moreover, the best-fit optimization  
32 used by the authors revealed that the missing source should be concentrated over the low  
33 latitudes in order to best fit the atmospheric data recorded at NOAA stations.

1 Using our “best guess” parameterization for NEMO-PISCES leads to relatively constant  
2 global OCS outgassing throughout the year, with a seasonal amplitude of only 10%. Tropical  
3 regions (30°S-30°N) emit the major part of the OCS, and represent up to 45% of the total  
4 emitted OCS towards the atmosphere. Tropical exchanges show almost no variation  
5 throughout the year. Northern and southern oceanic regions at mid- and high latitudes (higher  
6 than 30°N and 30°S, respectively) contribute to 20% and 35%, respectively, of the OCS  
7 global flux towards atmosphere each year (Fig A3).

8 Despite the consistency in terms of global OCS fluxes quantities and spatial distribution  
9 between best guess parameterizations of NEMO-PISCES and indirect oceanic source estimate  
10 from Berry et al. (2013), the simulated outgassing using NEMO-PISCES show a large  
11 envelope when using the different possible parameterizations. Most of them lead to much  
12 larger global flux estimates than previous studies, ranging between 573 and 3997 GgS yr<sup>-1</sup>.  
13 Higher estimates for OCS fluxes with NEMO-PISCES result from using hydrolysis constant  
14 from Kamyshny et al. (2003) or  $a_{350}$  calculation proposed in this present work. Kamyshny-  
15 based hydrolysis constant is not homogeneous with the choice of an Elliot-based hydrolysis  
16 constant used to determinate OCS dark-production by von Hobe et al. (2001), as implemented  
17 in NEMO-PISCES. Moreover, calculation of  $a_{350}$  proposed in this work was demonstrated to  
18 lead to large over-estimations of the  $a_{350}$  values compared with the observational data. Both  
19 parameterizations lead to very large estimates of OCS fluxes towards the atmosphere, which  
20 are not likely since they would lead to highly unbalanced atmospheric OCS budget.

21

## 22 **5 Conclusion**

23 At a global scale, the ocean is supposed to be the largest direct and indirect source of OCS to  
24 the atmosphere. Recent studies (Suntharalingam et al., 2008; Berry et al., 2013) pointed out  
25 the need to re-evaluate the global OCS sinks, signaling a possible underestimation in previous  
26 assessments. There is currently no trend in the atmospheric levels of OCS (Montzka et al.,  
27 2007), thus increased sinks have to be compensated by a source, currently missing from the  
28 global OCS budget. The recent inversion study of Berry et al. (2013) and previous  
29 Atmospheric Chemistry Experiment ACE observational analysis of Barkley et al. (2008) have  
30 suggested that a large part of this missing source should be ocean outgassing at low latitudes.  
31 Previous studies of the OCS production and removal processes in the ocean have only led to  
32 poor constraint of the potential global sea-air fluxes. Moreover, numerical simulations have

1 led to relatively small modeled global fluxes of OCS outgassed to the atmosphere. In this  
2 study we have selected different parameterizations for the most important OCS production  
3 and removal processes, which we then implemented in the 3D NEMO-PISCES ocean model.  
4 Simulated fluxes with this model showed a potential for large global OCS fluxes, with our  
5 best guess simulation reaching a net emission of OCS up to 800 GgS yr<sup>-1</sup>, much larger than  
6 previous estimated ranges. Moreover, the resulting spatial distribution of these fluxes  
7 supports the assumed key role of tropical regions, where warm marine waters can produce  
8 high levels of OCS with little organic matter. Our modeled ocean-atmosphere OCS fluxes  
9 were concentrated in the equatorial and subtropical regions, which accounted for half of the  
10 global OCS outgassing to the atmosphere. This result is in good agreement with the necessary  
11 distribution of the missing oceanic source of OCS that would be consistent with the  
12 atmospheric OCS concentration gradients (north south gradient for instance), measured at the  
13 different stations of the NOAA network. The uncertainties around OCS fluxes, however, will  
14 remain very large until a wide array of measurements focusing on the individual processes is  
15 available, to accurately calibrate the relative importance of each marine OCS production and  
16 removal process.

17

## 18 **Authors contribution**

19 S. Belviso and P. Peylin designed the experiments. T. Launois did the bibliography research  
20 for process parameterizations and developed the NEMO-PISCES specific OCS module code  
21 and performed the simulations with the help from L. Bopp. C. Fichot run tests with the  
22 SeaUV model that he developed, allowing comparison of OCS photo-production rates with  
23 the results obtained with NEMO-PISCES. T. Launois prepared the manuscript with  
24 contributions from all co-authors.

25

## 26 **Acknowledgements**

27 The authors wish to thank Elliott Campbell who shared simulation results from Kettle et al.  
28 (2002) and allowed the comparisons done in this work. We also thank Alina Gainusa-Bogdan  
29 for improving the manuscript.

## 30 **References**



- 1 Aumont, O., and L. Bopp, Globalizing results from ocean in situ iron fertilization studies,  
2 GLOBAL BIOGEOCHEM CY, 20, GB2017, doi:[10.1029/2005GB002591](https://doi.org/10.1029/2005GB002591), 2006
- 3 Barnes, I., Becker, K. H., Patroescu, I. The tropospheric oxidation of dimethyl sulfide: A new  
4 source of carbonyl sulfide. GEOPHYS RES LETT., 21(22), 2389-2392, 1997
- 5 Bopp L., Aumont O., Belviso S., Blain S, Modelling the effect of iron fertilization on  
6 dimethylsulphide emissions in the Southern Ocean. DEEP-SEA RES PT II, 55(5), 901-912,  
7 2008
- 8 Barkley M. P., Palmer P. I., Boone C. D., Bernath P. F. and Suntharalingam P., Global  
9 distributions of carbonyl sulfide in the upper troposphere and stratosphere. GEOPHYS RES  
10 LETT, 35, L14810, doi:[10.1029/2008GL034270](https://doi.org/10.1029/2008GL034270), 2008
- 11 Berry J., Wolf A., Campbell J. E., Baker I., Blake N., Blake D., Zhu, Z., A coupled model of  
12 the global cycles of carbonyl sulfide and CO<sub>2</sub>: A possible new window on the carbon cycle. J  
13 GEOPHYS RES-BIOGEO, 118(2), 842-852, 2013
- 14 Bricaud A., Babin M., Morel A., Claustre H., Variability in the chlorophyll-specific  
15 absorption coefficients of natural phytoplankton: Analysis and parameterization. J GEOPHYS  
16 RES-OCEANS, (1978–2012),100(C7), 13321-13332, 1995
- 17 Brühl C., Lelieveld J., Crutzen P. J., Tost H., The role of carbonyl sulphide as a source of  
18 stratospheric sulphate aerosol and its impact on climate. ATMOS CHEM PHYS, 12(3), 1239-  
19 1253, 2012
- 20 Campbell J. E., Carmichael G. R., Chai T., Mena-Carrasco M., Tang Y., Blake D. R., Stanier  
21 C. O., Photosynthetic control of atmospheric carbonyl sulfide during the growing  
22 season. SCIENCE, 322(5904), 1085-1088, 2008
- 23 Chin M., Davis D. D., A reanalysis of carbonyl sulfide as a source of stratospheric  
24 background sulfur aerosol. J GEOPHYS RES-OC ATMOS (1984–2012), 100(D5), 8993-  
25 9005, 1993
- 26 Cutter G. A., Cutter L. S., Filippino K. C., Sources and cycling of carbonyl sulfide in the  
27 Sargasso Sea. LIMNOL OCEANOGR, 49(2), 555-565, 2004
- 28 Elliott S., Lu E., Rowland F. S., Rates and mechanisms for the hydrolysis of carbonyl sulfide  
29 in natural waters. ENVIRON SCI TECHNOL, 23(4), 458-461, 1989
- 30 Farmer, CT., Moore, C.A., Zika, R.G. and Sikorski, R.J., Effects of low and high Orinoco  
31 river flow on the underwater light field of the Eastern Caribbean Basin, J GEOPHYS RES  
32 (2279-2288), 98, 1993
- 33 Ferek R. J., Andreae M. O., Photochemical production of carbonyl sulphide in marine surface  
34 waters, GLOBAL BIOGEOCHEM CY, 6(2), 175–183, 1984
- 35 Fichot C. G., Miller W. L., An approach to quantify depth-resolved marine photochemical  
36 fluxes using remote sensing: Application to carbon monoxide (CO)  
37 photoproduction. REMOTE SENS ENVIRON, 114(7), 1363-1377, 2010

- 1 Fichot C. G., Sathyendranath S., Miller W. L., SeaUV and SeaUVC: Algorithms for the  
2 retrieval of UV/Visible diffuse attenuation coefficients from ocean color. *REMOTE SENS*  
3 *ENVIRON*, 112(4), 1584-1602, 2008
- 4 Flöck O. R., Andreae M. O., Dräger M., Environmentally relevant precursors of carbonyl  
5 sulfide in aquatic systems. *MAR CHEM*, 59(1), 71-85, 1997
- 6 Johnson J. E., Harrison H., Carbonyl sulfide concentrations in the surface waters and above  
7 the Pacific Ocean. *J GEOPHYS RES-OC ATMOS* (1984–2012), 91(D7), 7883-7888, 1986
- 8 Kamyshny A., Goifman A., Rizkov D., Lev O., Formation of carbonyl sulfide by the reaction  
9 of carbon monoxide and inorganic polysulfides. *ENVIRON SCI TECHNOL*, 37(9), 1865-  
10 1872, 2003
- 11 Kettle, A. J., et al. (1999), A global database of sea surface dimethylsulfide (DMS)  
12 measurements and a procedure to predict sea surface DMS as a function of latitude, longitude,  
13 and month, *Global Biogeochem. Cycles*, 13(2), 399–444, doi:
- 14 Kettle A. J., Kuhn U., Hobe M. V., Kesselmeier J., Liss P. S., Andreae M. O., Comparing  
15 forward and inverse models to estimate the seasonal variation of hemisphere-integrated fluxes  
16 of carbonyl sulfide. *ATMOS CHEM PHYS*, 2(5), 343-361, 2002
- 17 Kloster S., Feichter J., Maier-Reimer E., Six K. D., Stier P., Wetzel P., DMS cycle in the  
18 marine ocean-atmosphere system? a global model study. *BIOGEOSCIENCES*, 3(1), 29-51,  
19 2006
- 20 Lana, A., et al. (2011), An updated climatology of surface dimethylsulfide concentrations and  
21 emission fluxes in the global ocean, *Global Biogeochem. Cycles*, 25, GB1004,  
22 doi:[10.1029/2010GB003850](https://doi.org/10.1029/2010GB003850)
- 23 Large W. G., Yeager S. G., The global climatology of an interannually varying air–sea flux  
24 data set, *CLIM DYNAM*, 33, 341–364, 2008
- 25 Madec G., NEMO ocean general circulation model reference manuel. Internal Report.  
26 LODYC/IPSL, Paris, 2008
- 27 Mihalopoulos N., Nguyen B. C., Putaud J. P., Belviso S., The oceanic source of carbonyl  
28 sulfide (COS). *ATMOS ENVIRON A-GEN*, 26(8), 1383-1394, 1992
- 29 Morel A., Optical modeling of the upper ocean in relation to its biogenous matter content  
30 (case I waters). *J GEOPHYS RES-OCEANS* (1978–2012), 93(C9), 10749-10768, 1988
- 31 Morel A., Gentili B., A simple band ratio technique to quantify the colored dissolved and  
32 detrital organic material from ocean color remotely sensed data. *REMOTE SENS*  
33 *ENVIRON*, 113(5), 998-1011, 2009
- 34 Montzka S. A., Calvert P., Hall B. D., Elkins J. W., Conway T. J., Tans P. P., Sweeney, C.,  
35 On the global distribution, seasonality, and budget of atmospheric carbonyl sulfide (COS) and  
36 some similarities to CO<sub>2</sub>. *J GEOPHYS RES-OC ATMOS* (1984–2012), 112(D9), 2007
- 37 Notholt J., Weisenstein D., Kuang Z., Rinsland C. P., Toon G. C., Rex M., Schrems O.,  
38 Composition of the upper tropical troposphere and its influence on the stratospheric aerosol  
39 formation. *EGS-AGU-EUG Joint Assembly* (Vol. 1, p. 4024), 2003

- 1 Para J., Coble P.G., Charrière B., Tedetti M., Fontana C., Sempéré R., Fluorescence and  
2 absorption properties of chromophoric dissolved organic matter (CDOM) in coastal surface  
3 waters of the northwestern Mediterranean Sea, influence of the Rhône River.  
4 *BIOGEOSCIENCES*, 7, 4083-4103, 2010
- 5 Preiswerk D., Najjar R. G., A global, open-ocean model of carbonyl sulfide and its air-sea  
6 flux. *GLOBAL BIOGEOCHEM CY*, 14(2), 585-598, 2000
- 7 Radford-Knoery J., Cutter G. A., Determination of carbonyl sulfide and hydrogen sulfide  
8 species in natural waters using specialized collection procedures and gas chromatography  
9 with flame photometric detection. *ANAL CHEM*, 65(8), 976-982, 1993
- 10 Rasmussen R. A., Khalil M. A. K., Hoyt S. D., The oceanic source of carbonyl sulfide  
11 (OCS). *ATMOS ENVIRON* (1967), 16(6), 1591-1594, 1982
- 12 Suntharalingam P., Kettle A. J., Montzka S. M., Jacob D. J., Global 3-D model analysis of the  
13 seasonal cycle of atmospheric carbonyl sulfide: Implications for terrestrial vegetation  
14 uptake. *GEOPHYS RES LETT*, 35(19), 2008
- 15 Tedetti M., Sempéré R., Penetration of ultraviolet radiation in the marine environment. A  
16 review. *PHOTOCHEM PHOTOBIOLOG*, 82(2), 389-397, 2006
- 17 Uher G., Distribution and air-sea exchange of reduced sulphur gases in European coastal  
18 waters. *ESTUAR COAST SHELF S*, 70(3), 338-360, 2006
- 19 Uher G., Andreae M. O., Photochemical production of carbonyl sulfide in North Sea water: A  
20 process study. *LIMNOL OCEANOGR*, 42(3), 432-442, 1997
- 21 Ulshöfer V. S., Uher G., Andreae M. O., Evidence for a winter sink of atmospheric carbonyl  
22 sulfide in the northeast Atlantic Ocean. *GEOPHYS RES LETT*, 22(19), 2601-2604, 1995
- 23 Ulshöfer V. S., Flock O. R., Uher G., Andreae M. O., Photochemical production and air-sea  
24 exchange of carbonyl sulfide in the eastern Mediterranean Sea. *MAR CHEM*, 53(1), 25-39,  
25 1996
- 26 Von Hobe M., Cutter G. A., Kettle A. J., Andreae M. O., Dark production: A significant  
27 source of oceanic COS. *J GEOPHYS RES-OCEANS* (1978-2012), 106(C12), 31217-31226,  
28 2001
- 29 Von Hobe M., Najjar R. G., Kettle A. J., Andreae M. O., Photochemical and physical  
30 modeling of carbonyl sulfide in the ocean. *J GEOPHYS RES-OCEANS* (1978-  
31 2012), 108(C7), 2003
- 32 Wanninkhof R., Relationship between wind speed and gas exchange over the ocean. *J*  
33 *GEOPHYS RES-OCEANS* (1978-2012), 97(C5), 7373-7382, 1992
- 34 Watts S. F., The mass budgets of carbonyl sulfide, dimethyl sulfide, carbon disulfide and  
35 hydrogen sulfide. *ATMOS ENVIRON*, 34(5), 761-779, 2000
- 36 Weiss P. S., Johnson J. E., Gammon R. H., Bates T. S., Reevaluation of the open ocean source  
37 of carbonyl sulfide to the atmosphere. *J GEOPHYS RES-OC ATMOS* (1984-  
38 2012), 100(D11), 23083-23092, 1995a

- 1 Weiss P. S., Andrews S. S., Johnson J. E., Zafiriou O. C., Photoproduction of carbonyl sulfide  
2 in South Pacific Ocean waters as a function of irradiation wavelength. *GEOPHYS RES*  
3 *LETT*, 22(3), 215-218, 1995b
- 4 Wohlfahrt G., Brilli F., Hörtnagl L., Xu X., Bingemer H., Hansel A., Loreto F., Carbonyl  
5 sulfide (COS) as a tracer for canopy photosynthesis, transpiration and stomatal conductance:  
6 potential and limitations†. *PLANT CELL ENVIRON*, 35(4), 657-667, 2012
- 7 Xu X., Bingemer H. G., Georgii H. W., Schmidt U., Bartell, U., Measurements of carbonyl  
8 sulfide (COS) in surface seawater and marine air, and estimates of the air-sea flux from  
9 observations during two Atlantic cruises. *J GEOPHYS RES-OC ATMOS* (1984–  
10 2012), 106(D4), 3491-3502, 2001
- 11 Zepp R. G., Andreae M. O., Factors affecting the photochemical production of carbonyl  
12 sulfide in seawater. *GEOPHYS RES LETT*, 21(25), 2813-2816, 1994

13

14

15

16

17

18

19

20

21

22

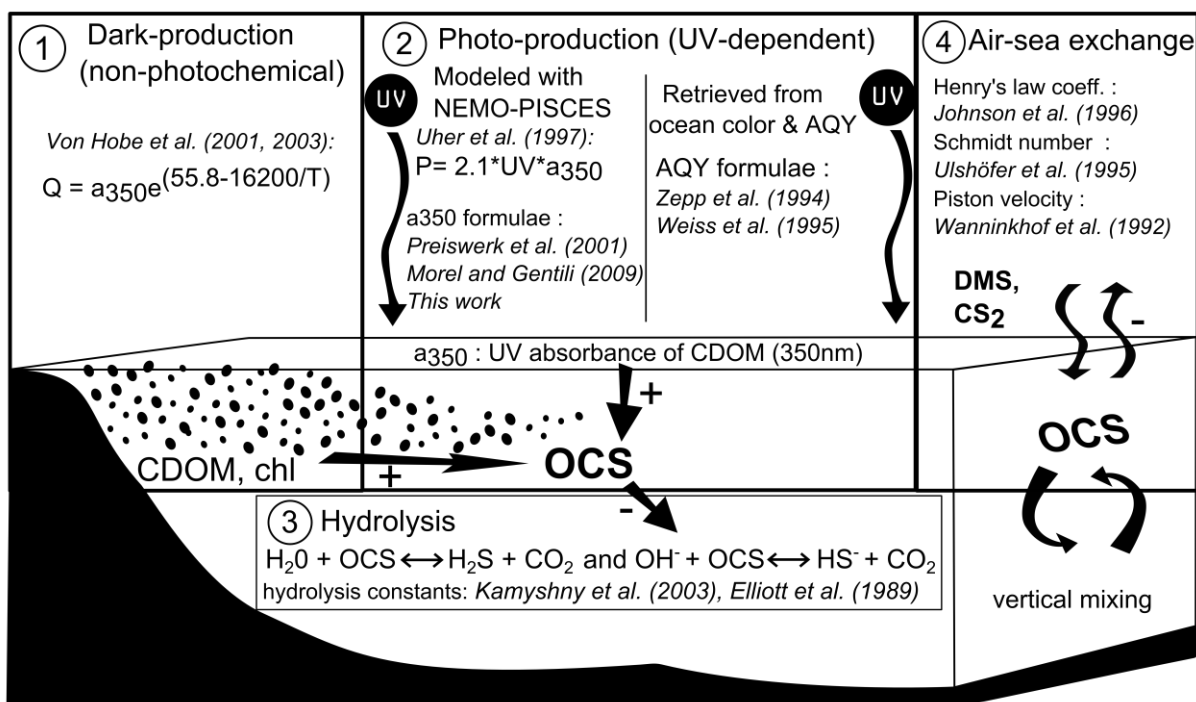
23

24

25

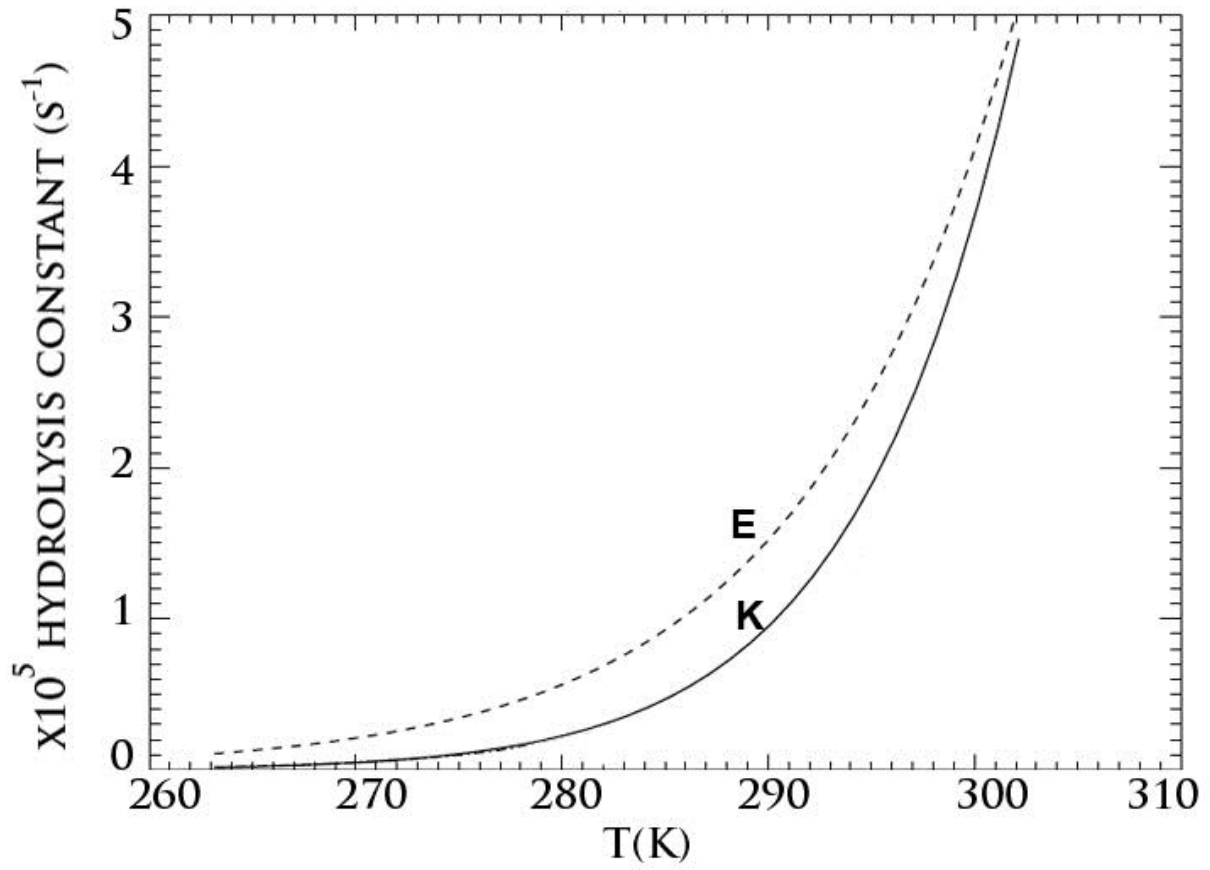
26

27



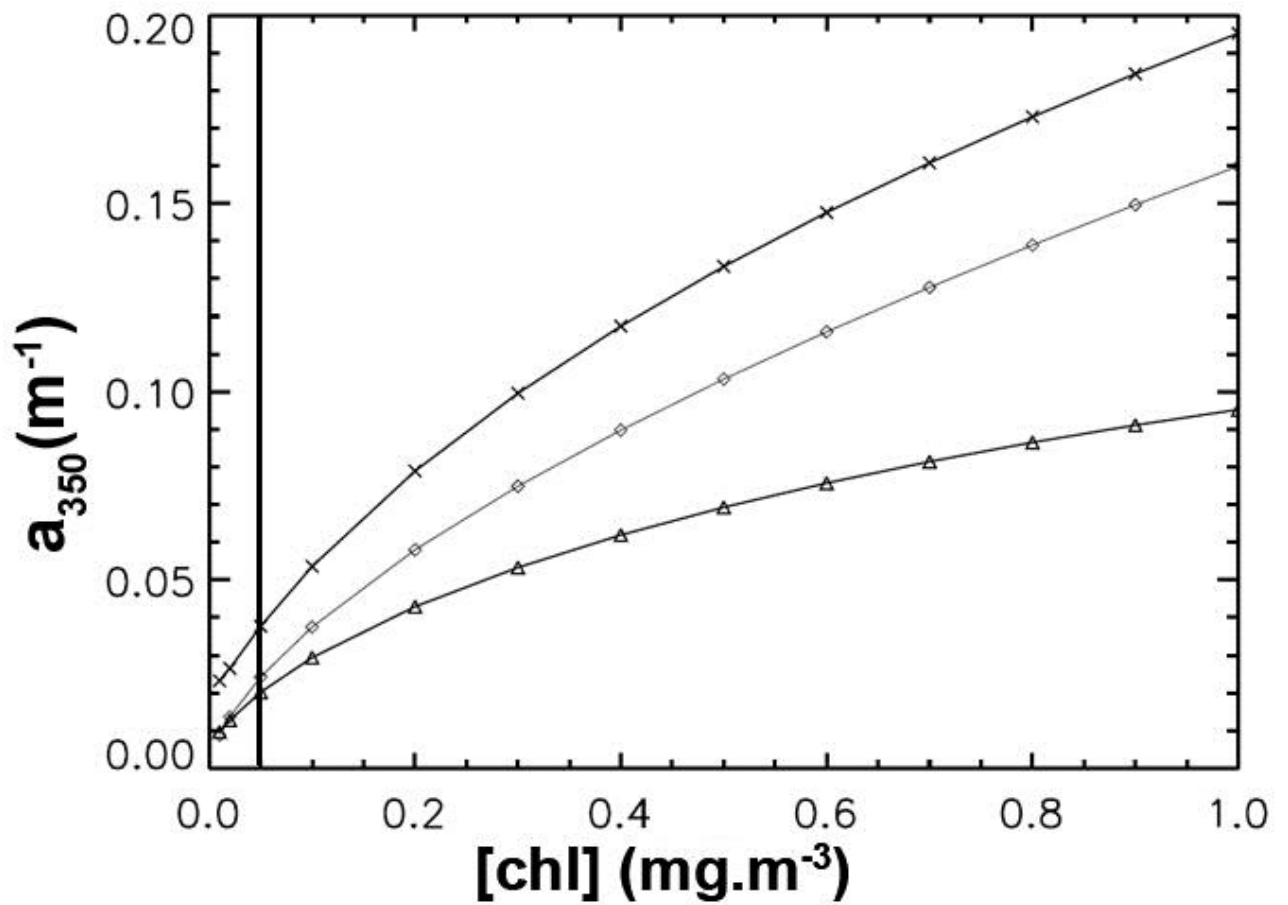
1

2 Figure 1: Main production and removal processes implemented in the NEMO-PISCES  
 3 OGCM to simulate the marine OCS cycle: dark-production, photo-production and hydrolysis.  
 4 Of central importance is the UV absorption coefficient at 350 nm of chromophoric dissolved  
 5 organic matter (CDOM) which is derived from modeled Chl concentrations using three  
 6 different relationships linking  $a_{350}$  to Chl. The simulated photo-production rates of OCS were  
 7 evaluated independently using the model of Fichot and Miller (2010) and published apparent  
 8 quantum yields (AQY). Aqueous OCS is removed by hydrolysis (two different formulations  
 9 of the hydrolysis rate are used), lost or absorbed at the air-sea interface and mixed both  
 10 vertically and horizontally. Studies relevant for sensitivity tests and model parameterization  
 11 presented in this paper are displayed in *italics*. Oceans also emit DMS and CS<sub>2</sub> which are later  
 12 oxidized in OCS in the atmosphere. These indirect sources of OCS are not detailed in the  
 13 present study.



1  
2  
3  
4  
5  
6  
7  
8  
9  
10  
11

Figure 2: Temperature dependence of hydrolysis rates implemented in NEMO-PISCES. The relationships are represented for pH = 8.2, and taken from Elliott et al. (1989) (E, dashed line) or Kamyshny et al. (2003) (K, solid line).

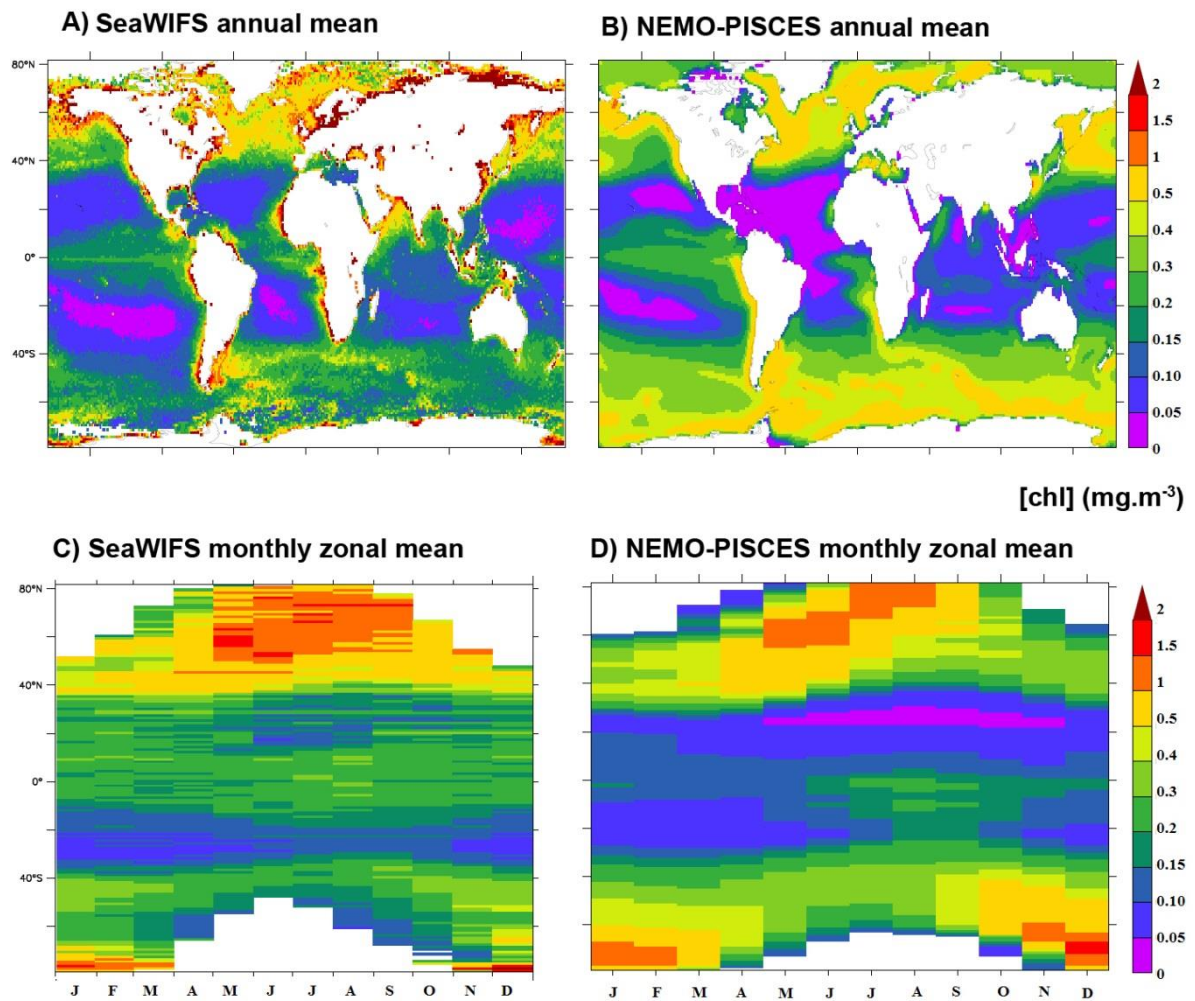


1

2 Figure 3: Relationships implemented in the NEMO-PISCES model between UV absorption  
 3 coefficients for CDOM at 350 nm and chlorophyll concentrations. The 3 respective  
 4 relationships are from Morel and Gentili (2009) (diamonds), Preiswerk et al. (2000)  
 5 (triangles) or issued from this study, based on MODIS-Aqua ocean color (crosses).  
 6 Chlorophyll concentrations in NEMO-PISCES have a fixed minimal value of 0.05 mg.m<sup>-3</sup>  
 7 (thick vertical line).

8

9

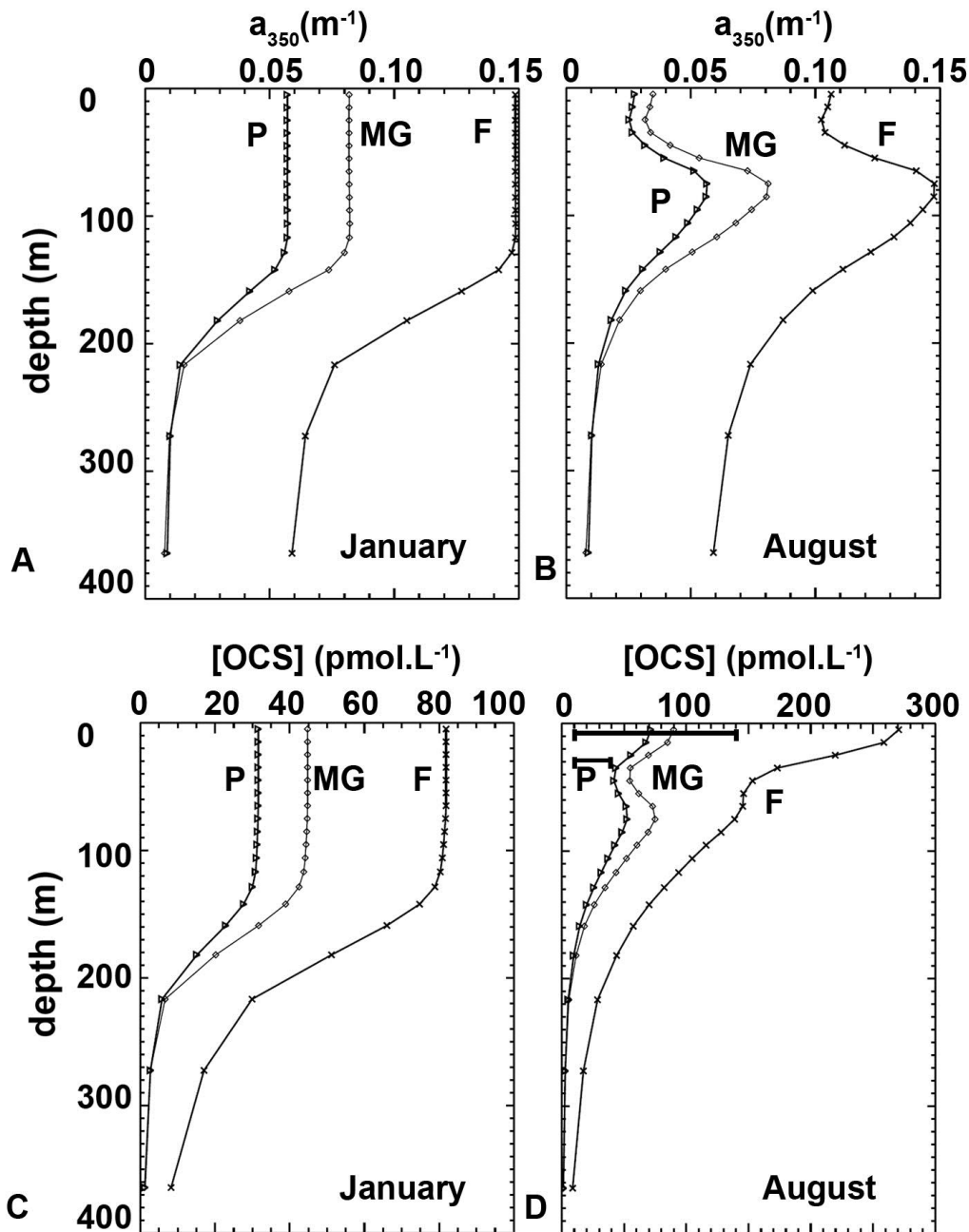


1

2 Figure 4: Comparison of remotely sensed observations of chlorophyll (left panels) with  
 3 simulations performed using the NEMO-PISCES model (right panels). Top panels (a, b)  
 4 represent maps of annual mean chlorophyll concentration ( $\text{mg}\cdot\text{m}^{-3}$ ). Bottom panels (c, d)  
 5 represent latitude-time maps of chlorophyll.

6

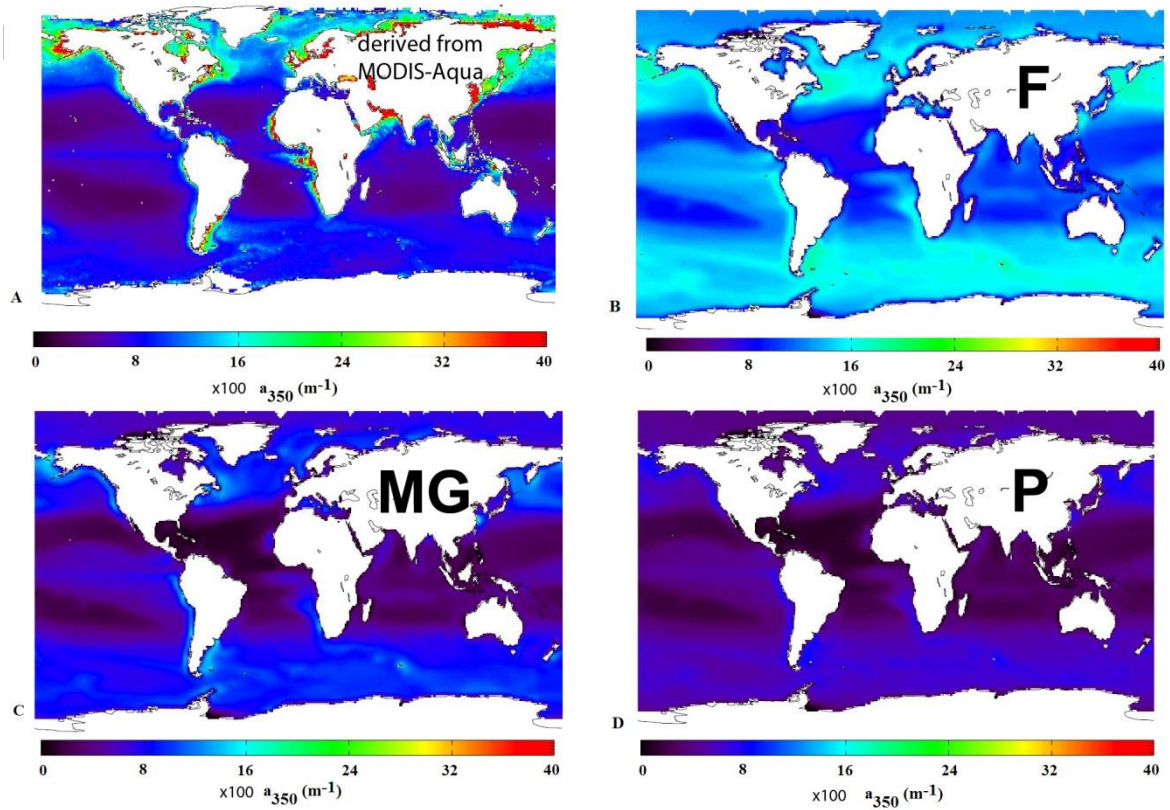




1

2 Figure 5: Monthly mean vertical profiles of  $a_{350}$  (top row) and OCS concentration (bottom  
 3 row) in January (left column) and August (right column) simulated by NEMO-PISCES in a 1-  
 4 D run at the Bermuda Atlantic Time Series (BATS) site. The thick lines on figure D cover the  
 5 range between minimal and maximal values as measured by Cutter et al. (2004). The different  
 6  $a_{350}$  profile are calculated using the formulations of Morel and Gentili (2009) (MG,  
 7 diamonds), Preiswerk et al. (2000) (P, triangles) or based on MODIS-*aqua* data (F, black  
 8 line). Symbols used on OCS concentration profile on bottom row indicate which  $a_{350}$ -  
 9 chlorophyll relation was used in the simulation.

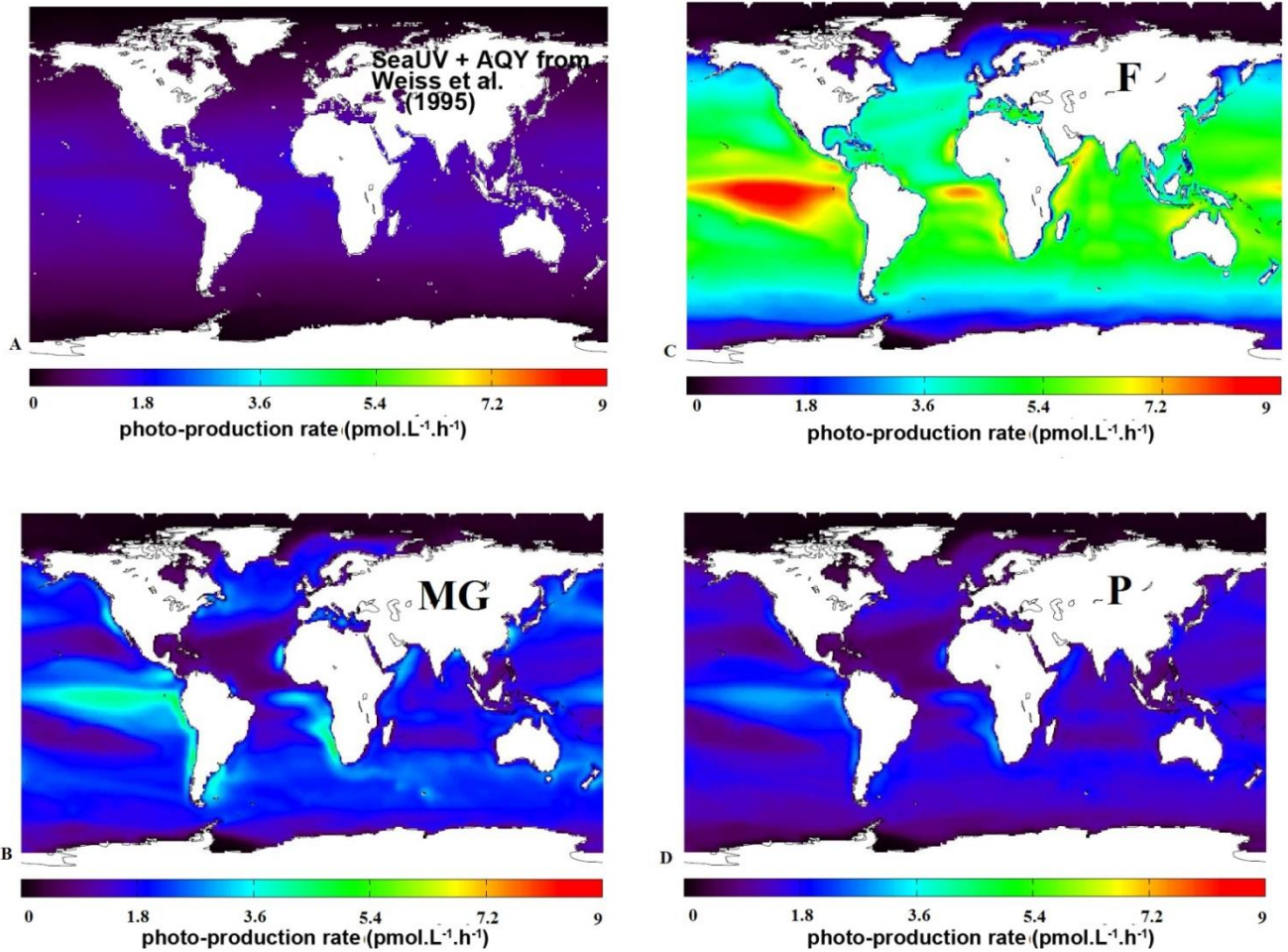
10



1

2 Figure 6: Comparison between annual mean surface absorption coefficient of CDOM at 350  
 3 nm: (A) retrieved from MODIS-*Aqua* satellites data, using SeaUV model (Fichot et al., 2008)  
 4 and  $a_{320}/K_{d320}$  ratio from Fichot and Miller (2010) and  $a_{350}$  maps simulated with the NEMO-  
 5 PISCES model using the relation described in Morel and Gentili (2009) (MG, panel C),  
 6 Preiswerk et al. (2000) (P, panel D) or proposed in this work (F, panel B).

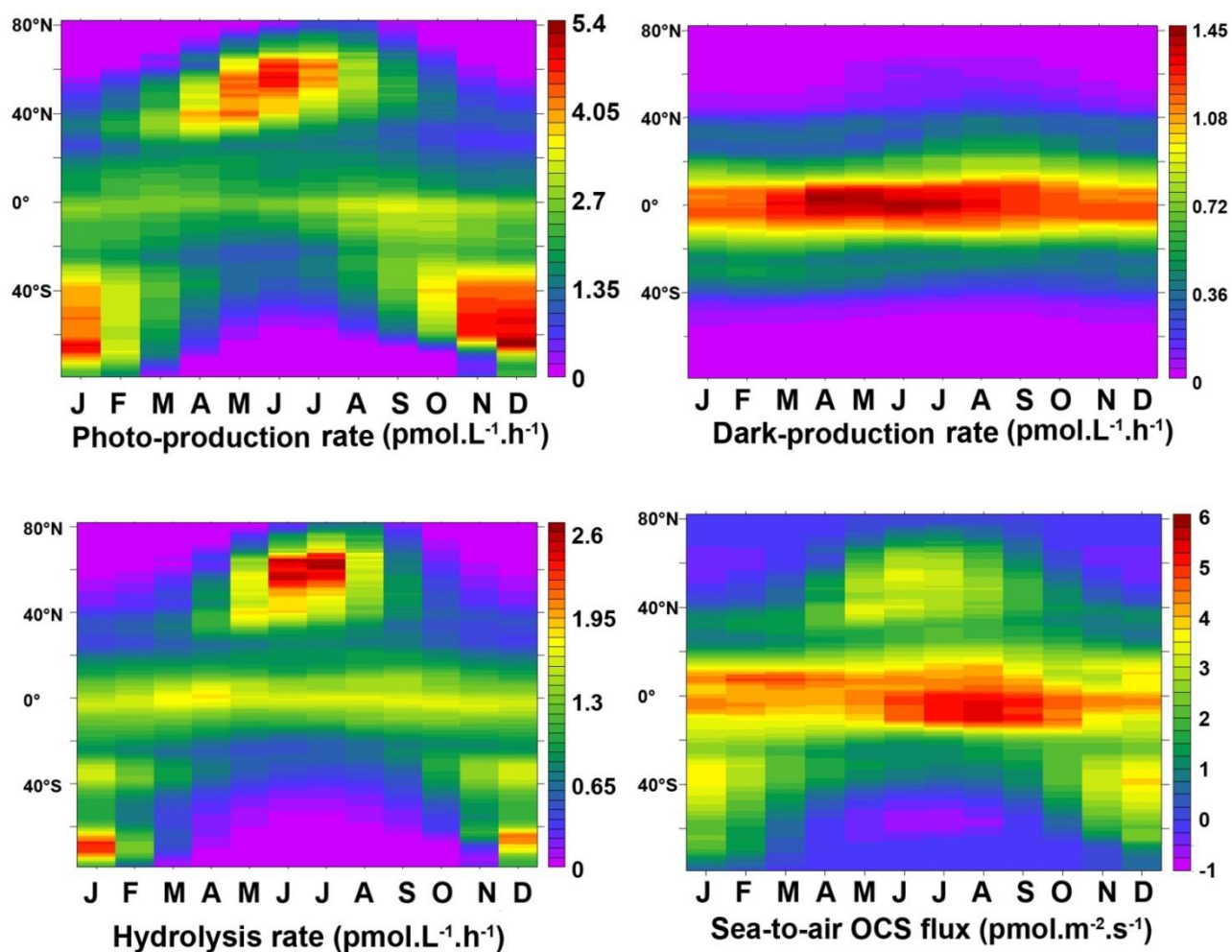
7



1

2 Figure 7: Annual mean photo-production rates integrated over the entire water column  
 3 simulated with the photochemical model of Fichot and Miller (2010) and using the apparent  
 4 quantum yield of Weiss et al (1995a) (panel A). Comparison with annual mean photo-  
 5 production rates integrated over the entire water column simulated with the NEMO-PISCES  
 6 model using  $a_{350}$  formulations from Morel and Gentili (2009) (panel C), Preiswerk et al.  
 7 (2000) (panel D) or proposed in this study (panel B).

8



1

2 Figure 8: Latitude-time plots comparing relative importance of individual processes for OCS  
 3 production (top row) and removal (bottom row) in NEMO-PISCES surface layer. Sea-air  
 4 exchanges are displayed in bottom right panel are displayed with positive fluxes when OCS is  
 5 outgassed towards the atmosphere. All runs were performed using Morel and Gentili (2009)  
 6 formulation to calculate  $a_{350}$  and Elliott et al. (1989) formulation of hydrolysis constant.

7

8

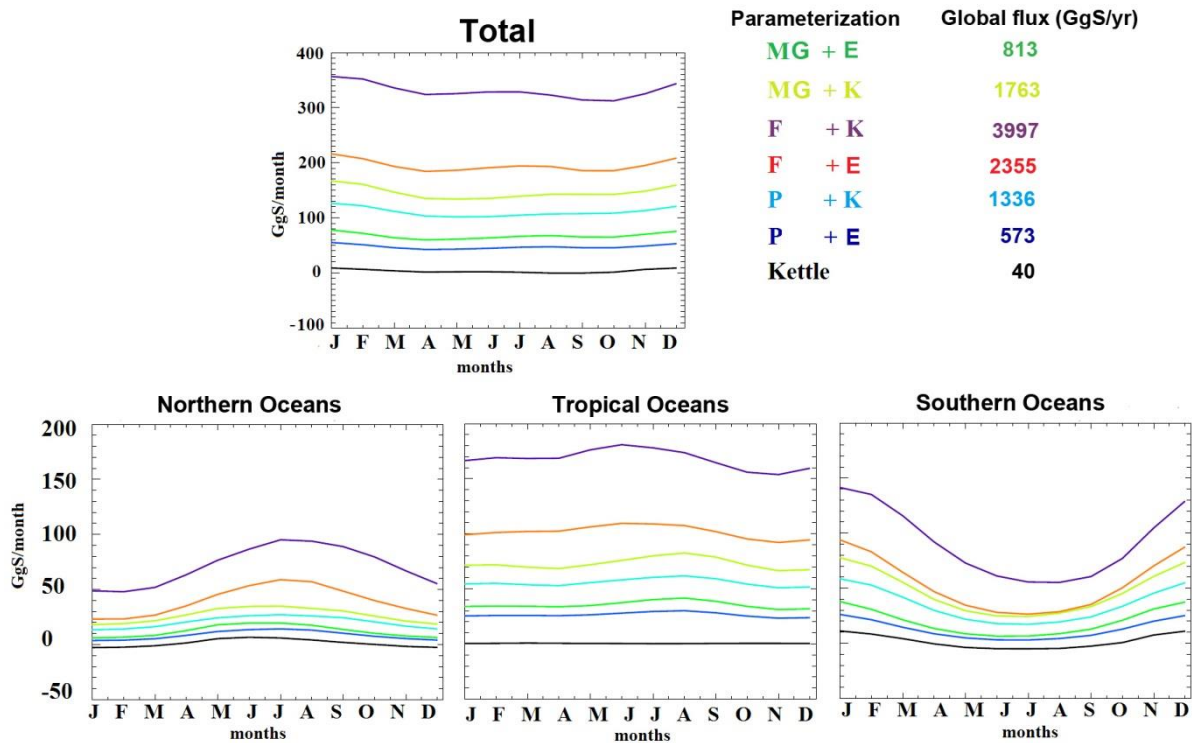
9

10

11

12

13



1

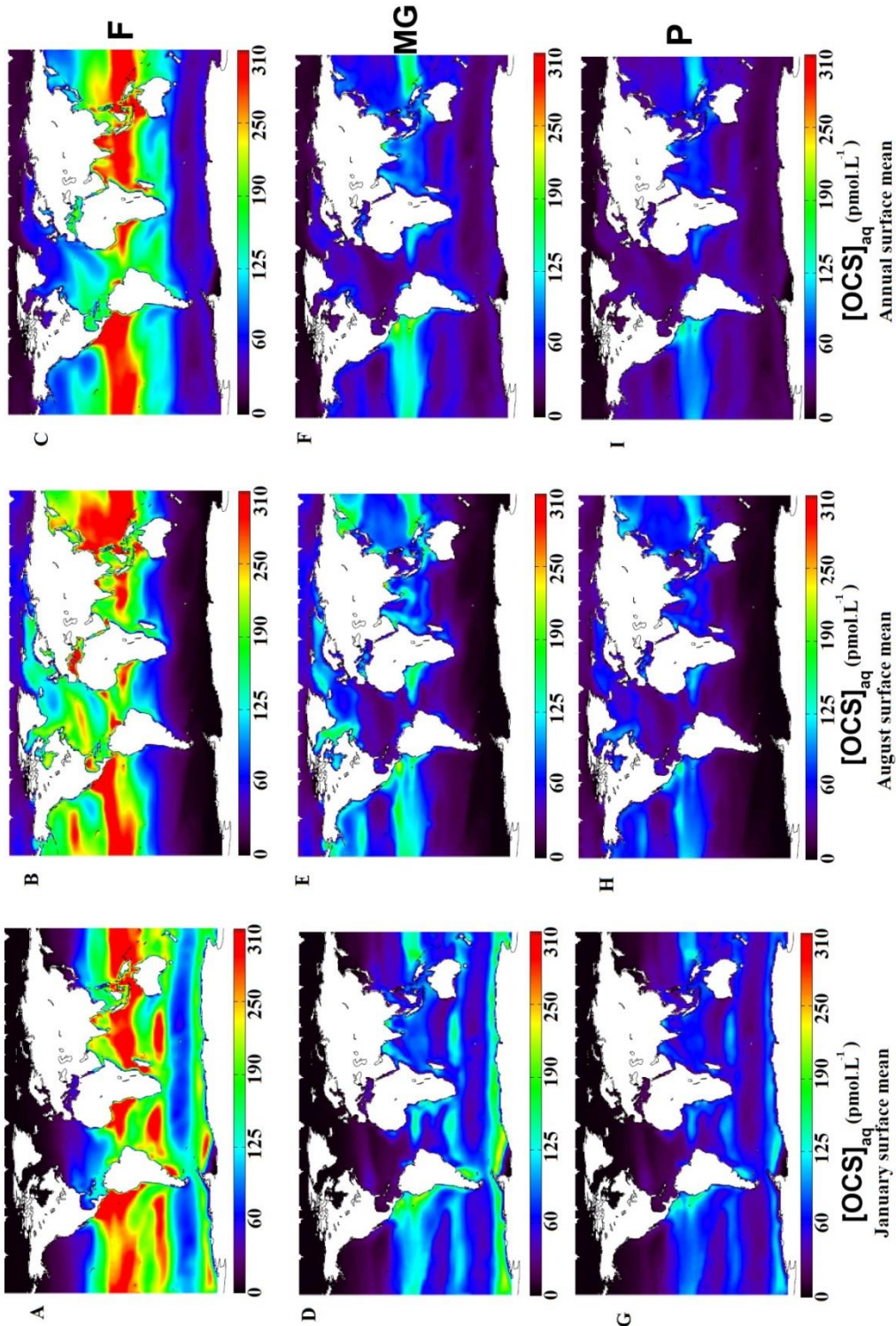
2 Figure 9: Global and regional monthly mean sea-air fluxes for 6 different parameterizations of  
 3 the NEMO-PISCES model. Kettle et al. 2002 (black line) is shown as a reference. Each  
 4 colored line represents a set of parameters: first name refers to the equation used to calculate  
 5 the UV absorption coefficient of CDOM at 350 nm and the second name refers to the  
 6 hydrolysis constant formulation. Global fluxes on top row, Northern Oceans (30°N-90°N,  
 7 bottom left), Tropical region (30°S-30°N, bottom center), Southern Oceans (30°S-90°S,  
 8 bottom right). F:  $a_{350}$  relation assembled in this study; MG:  $a_{350}$  relation from Morel and  
 9 Gentili (2009); P:  $a_{350}$  relation from Preiswerk et al. (2000); E: hydrolysis constant from  
 10 Elliott et al. (1989); K: hydrolysis constant from Kamyshny et al. (2003)

11

12

13

14



1

2 Figure 10: Monthly mean surface OCS concentrations for January (left column), August  
 3 (central column) and annual mean (right column) simulated with NEMO-PISCES. The three  
 4 simulations differ in the relationship used to calculate  $a_{350}$  from chlorophyll: MODIS *Aqua*-  
 5 derived, proposed in this study (F, upper row), from Preiswerk et al. (2000)(P, central row) or  
 6 Morel and Gentili (2009)(MG, lower row).

7

1  
2  
3  
4  
5  
6  
7  
8  
9  
10  
11  
12  
13  
14  
15  
16  
17  
18  
19  
20  
21  
22  
23  
24

Table 1: Annual global photo-production of OCS in the entire water column simulated with the NEMO-PISCES model (using the three different  $a_{350}$  formulations presented in this paper) or with the photochemical model derived from Fichot and Miller (2010) (FM in the table)(using two different apparent quantum yields estimates). F:  $a_{350}$  parameterization assembled in this work; MG:  $a_{350}$  parameterization presented in Morel and Gentili (2009); P:  $a_{350}$  parameterization presented in Preiswerk et al. (2000).

<b>Parameterization used in the runs</b>	<b>Total photo-produced OCS in the entire water column (GgS yr<sup>-1</sup>)</b>
NEMO-PISCES + F	4540
NEMO-PISCES + MG	1910
NEMO-PISCES + P	1390
FM + AQY from Weiss et al. (1995a)	876
FM + AQY from Zepp et al. (1994)	5500

1  
2  
3  
4  
5  
6  
7  
8  
9

10 Table 2: Yearly global OCS flux emitted from ocean to the atmosphere (in GgS yr<sup>-1</sup>)  
 11 depending on the different parameterizations presented in previous work and in this work. F:  
 12 a<sub>350</sub> parameterization presented in this work; MG: a<sub>350</sub> parameterization presented in Morel  
 13 and Gentili (2009); P: a<sub>350</sub> parameterization presented in Preiswerk et al. (2000).

Study	Method		Annual flux (GgS yr <sup>-1</sup> )
<b>Interpolation of observations</b>			
Chin and Davis (1993)	sea surface OCS supersaturation ratios <sup>a</sup>		200 to 900
Watts (2000)	OCS surface concentration <sup>b</sup>		300*
<b>Forward modeling</b>			
	<b>AQY/a<sub>350</sub></b>	<b>hydrolysis constant</b>	
Kettle et al. (2002) <sup>c</sup>	AQY	Elliott et al., 1989	40**
Berry et al. (2013) <sup>d</sup>	from Kettle et al. (2002)	from Kettle et al. (2002)	736
This work standard run	a <sub>350</sub> from MG	Elliott et al. (1989)	813

14 <sup>a</sup>sea surface OCS supersaturation ratios from open oceans, upwelling zones and coastal  
 15 regions

16 <sup>b</sup>OCS surface concentration from estuarine, coastal and open ocean environments

17 <sup>c</sup>Based on UV irradiance and apparent quantum yields from the literature. Lowest and highest  
 18 boundaries of the estimates correspond to the lowest and highest AQY used.

19 <sup>d</sup>136 GgS yr<sup>-1</sup> taken from Kettle upper estimate. Added source of 600 GgS yr<sup>-1</sup> necessary to  
 20 equilibrate the global budget.

21 \* 100 GgS yr<sup>-1</sup> from open ocean and 200 GgS yr<sup>-1</sup> from coastal shores



1 \*\* uncertainty range: between  $-110 \text{ GgS yr}^{-1}$  and  $+190 \text{ GgS yr}^{-1}$

2

3

4

5

6

7

8

9